JGR Oceans

RESEARCH ARTICLE
10.1029/2025JC022622

Key Points:

- Salinity and temperature frontal systems jointly control sediment trapping and deposition in energetic shelf seas
- Despite seasonal variations in the frontal systems, persistent sedimentation occurs in the mud depocenter
- Sedimentation on the mud depocenter is promoted by storms and floods

Supporting Information:

Supporting Information may be found in the online version of this article.

Correspondence to:

J. Chen and W. Zhang,
jiayue.chen@hereon.de;
wenyan.zhang@hereon.de

Citation:

Chen, J., Zhang, W., Porz, L., Arlinghaus, P., Hanz, U., Holtappels, M., & Schrum, C. (2025). Physical mechanisms of sediment trapping and deposition on spatially confined mud depocenters in high-energy shelf seas. *Journal of Geophysical Research: Oceans*, *130*, e2025JC022622. https://doi.org/10.1029/2025JC022622

Received 10 MAR 2025
Accepted 24 JUN 2025

Author Contributions:

Conceptualization: Jiayue Chen, Wenyan Zhang, Corinna Schrum
Data curation: Jiayue Chen, Lucas Porz, Peter Arlinghaus, Ulrike Hanz, Moritz Holtappels
Formal analysis: Jiayue Chen, Wenyan Zhang, Lucas Porz, Corinna Schrum
Funding acquisition: Wenyan Zhang, Corinna Schrum
Investigation: Jiayue Chen, Ulrike Hanz
Methodology: Jiayue Chen, Wenyan Zhang, Lucas Porz, Corinna Schrum
Project administration: Wenyan Zhang, Corinna Schrum

Physical Mechanisms of Sediment Trapping and Deposition on Spatially Confined Mud Depocenters in High-Energy Shelf Seas

Jiayue Chen[1], Wenyan Zhang[1], Lucas Porz[1], Peter Arlinghaus[1], Ulrike Hanz[2], Moritz Holtappels[2,3], and Corinna Schrum[1,4]

[1]Institute of Coastal Systems—Analysis and Modeling, Helmholtz-Zentrum Hereon, Geesthacht, Germany, [2]Alfred Wegener Institute Helmholtz Centre for Polar and Marine Research, Bremerhaven, Germany, [3]MARUM—Center for Marine Environmental Sciences, University of Bremen, Bremen, Germany, [4]Center for Earth System Sustainability, Institute of Oceanography, Universität Hamburg, Hamburg, Germany

Abstract Mud depocenters in shelf seas serve as a key element in the source-to-sink system of sediment transport on the Earth surface. Despite their undoubtful importance, physical mechanisms for formation, sediment budgeting, and cycling of localized depocenters in high-energy environments remain largely unknown. This study aims to fill the knowledge gap by focusing on sediment dynamics related to a localized mud depocenter in the southern North Sea. By combining field observation with 3-dimensional numerical simulations, we analyzed hydrodynamics and sediment dynamics over a 3-year period. Our results indicate a persistent transport of fine-grained sediments toward the depocenter and subsequent trapping resulting in accumulation, with distinct seasonal and spatial variations in the net depositional rate. The interaction of wind-driven coastal circulation with two distinct frontal systems—a salinity front and a tidal mixing front—emerges as a key mechanism of sediment dynamics. While the salinity front remains persistently over the depocenter, promoting sediment deposition year-round, the tidal mixing front appears primarily in summer, limiting sediment deposition. Sediment flows from offshore and along the coast provide major supply to the depocenter, while contemporary riverine sediment outflows contribute only marginally. Southwesterly winds enhance erosion and northerly winds promote deposition in the depocenter. Additionally, short-term extreme events significantly contribute to annual net sedimentation. Our work highlights the critical importance of frontal systems and extreme events for mud depocenter development in high-energy shelf seas.

Plain Language Summary Coastal environments constantly change as water moves sediment, forming areas where mud accumulates, known as mud depocenters. However, the processes controlling development of these deposits are not fully understood. This study examines a mud depocenter in the southern North Sea to understand how ocean currents, river flow, tides, and wind influence sediment movement. We found that two key oceanic density fronts—a riverine salinity front and a tidal mixing front—play a crucial role in trapping sediment. The salinity front is present year-round, while the tidal front appears mainly in summer. The contrasting effects of these two fronts lead to higher sediment accumulation in winter. Wind direction also affects deposition, with southwesterly winds causing erosion and northerly winds promoting deposition. Extreme events like storms and river floods significantly increase sedimentation over short periods. Our results highlight the critical importance of frontal systems and extreme events that shape coastal sedimentation in high-energy shelf seas. Understanding these processes is especially important for predicting coastal changes, as human activities may also influence sediment dynamics.

1. Introduction

Mud depocenters in shelf seas represent the major proximal-marine sinks for fine-grained sediment delivered from the land (Hanebuth et al., 2015). When continental shelves are extensively inundated under present-day sea level, a substantial portion of land-supplied sediment enters the ocean and is retained in mud depocenters, making these depocenters a crucial part in the source-to-sink routing system along the river-estuary-ocean continuum (Durrieu De Madron et al., 2000; Severinghaus & Brook, 1999; Weight et al., 2011; Weltje & Brommer, 2011). Although reduced bottom current strength is a prerequisite for deposition of fine-grained sediments, formation and maintenance of mud depocenters in shelf seas are influenced by complex environmental conditions. Five major mechanisms related to the formation and dynamics of mud depocenters have been identified according to a

Resources: Jiayue Chen, Wenyan Zhang, Corinna Schrum
Software: Jiayue Chen, Lucas Porz, Peter Arlinghaus
Supervision: Wenyan Zhang, Corinna Schrum
Validation: Jiayue Chen, Lucas Porz, Peter Arlinghaus, Ulrike Hanz, Moritz Holtappels
Visualization: Jiayue Chen, Wenyan Zhang, Lucas Porz, Peter Arlinghaus, Ulrike Hanz
Writing – original draft: Jiayue Chen
Writing – review & editing: Jiayue Chen, Wenyan Zhang, Lucas Porz, Peter Arlinghaus, Ulrike Hanz, Moritz Holtappels, Corinna Schrum

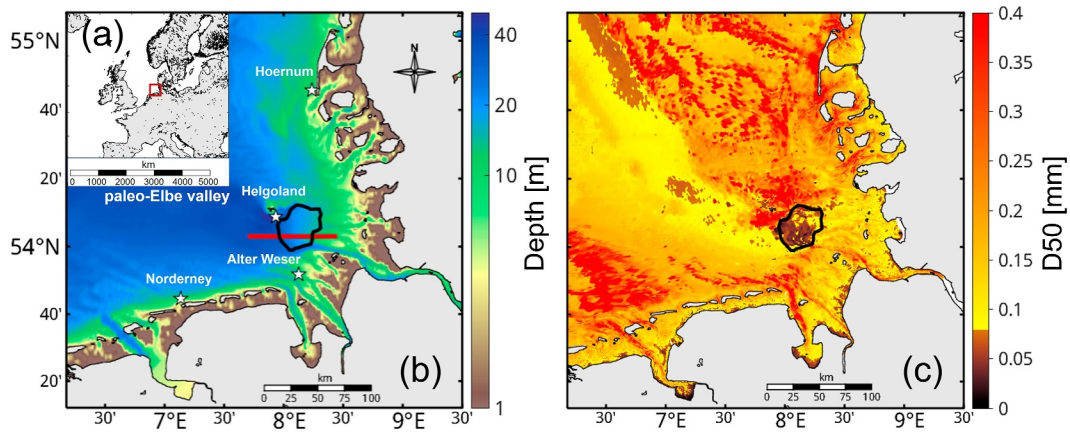

Figure 1. (a) Model domain and (b) the focus study area in the German Bight. The black polygon in (b) marks the Helgoland mud area (HMA) with mud content >50% identified by Hebbeln et al. (2003). Stars indicate the location of tide gauges. The red bold line indicates the transect used in data analysis. (c) Distribution of the median sediment diameter (D50) in the surface seabed at 100 × 100 m resolution derived from the EasyGSH database (Sievers et al., 2020).

review by Porz et al. (2021), including (a) sediment convergence by density gradients associated with frontal systems, (b) cross-shore bottom transport through gravity flows, (c) bed load deposition forming laminated bedding under energetic flow conditions, (d) internal wave-induced resuspension and dispersal, and (e) anthropogenic influences such as structure- or bottom trawling-induced resuspension and redistribution or sediment management. In particular, sediment convergence caused by density fronts associated with freshwater, thermohaline, tidal mixing or upwelling has been identified as the major mechanism for formation of certain types of mud depocenters (Castaing et al., 1999; Geyer et al., 2004; Kämpf, 2019; Liu et al., 2018; W. Zhang et al., 2016).

The predominance of each mechanism leading to mud depocenter development depends to a large degree on the hydrodynamic setting and on the timescales considered. Continuous sediment deposition mostly occurs in persistently quiescent hydrodynamic conditions such as in fjords (Addison et al., 2013), semi- or completely enclosed water bodies (Jokinen et al., 2015), and regions under the influence of gyres/circulations (Sprenk et al., 2014), leading to the deposition of finely laminated sediments. Continual resuspension-deposition cycles occur under dynamic hydrodynamic conditions, resulting in intermittent phases of deposition or erosion (Walsh & Nittrouer, 1999). Episodic sedimentation and erosion are triggered by events such as river floods and atmospheric storms (Collins et al., 2017).

In high-energy coastal and continental shelf environment characterized by strong tidal currents, wind waves and/or coastal currents, formation of mud depocenters requires mechanisms that not only promote deposition of fine-grained sediments but also trap them (W. Zhang et al., 2016). Fronts have been unraveled to provide such a mechanism in estuaries (Burchard et al., 2018; Ma et al., 2024; Ralston et al., 2012) and coastal waters (Castaing et al., 1999; Liu et al., 2018). On the other hand, fronts in open coastal and shelf waters exhibit large spatio-temporal variability and a knowledge gap exists in bridging the scales between the frontal dynamics and long-term development of mud depocenters (Dong et al., 2020; Porz et al., 2021; Shi et al., 2019). An example is from the existing understanding of development of a spatially confined mud depocenter, so-called the Helgoland mud area (HMA hereafter), in the German Bight (Figure 1). Studies based on mineral analysis indicated that the major sediment source of the HMA is from the Elbe River (Pache et al., 2008). A recent study found that the southern part of the HMA is characterized by a higher sedimentation rate than other parts and the organic carbon deposited in this part is mainly of terrigenous origin, whereas organic carbon deposited in the central and northern parts of the HMA exhibits a mixture of marine and terrigenous material (Müller et al., 2024). However, other studies revealed that most of the fine-grained sediment from the present-day Elbe River cannot reach the HMA and is rather deposited in the estuary due to the impact of tidal pumping and estuarine circulation (Burchard et al., 2018; Lenz et al., 2024; Weilbeer, 2014). Regularly dredged material from the Elbe estuary and the Hamburg harbor, which has been dumped in the German Bight for several decades may also influence the sediment composition in the HMA (Irion et al., 1987). It remains undetermined to what extent a direct transport from the present-day Elbe River contributes to the deposition in the HMA. Moreover, the spatial heterogeneity of

sediment composition in the HMA cannot be explained by existing studies and the driving mechanism remains unexplored.

This paper aims to address the challenges in bridging the spatiotemporal scales in the development of spatially confined mud depocenters in high-energy coastal environment. We present a case study of the German Bight in the southern North Sea by combining field observations with simulation results from a three-dimensional coastal ocean model. We simulated hydrodynamics and sediment dynamics in the study area for three consecutive years characterized by distinct seasonal and annual variations in the freshwater discharge and wind forcing that significantly modulate the hydrodynamic regime and sediment transport pathways. Analysis of the simulations allows us to disentangle the respective roles of involved driving forces as well as their interactions in the development of a spatially confined mud depocenter. The major sediment sources and the relative importance of different modes of sediment supply for the mud depocenter were also investigated. Implications for understanding development of mud depocenters in global shelf seas were then discussed.

2. Data and Method

2.1. Study Area

The study area is the German Bight located in the southern North Sea (Figure 1). This area is characterized by shallow water with water depth of its major part less than 40 m. This region is subject to a strong combined action of wind, astronomical tides, and river runoff (Becker et al., 1992). Tidal currents are dominated by semidiurnal constituents (M2 and S2) with speed of up to ∼2 m s^{-1} (Schrum, 1997). Seabed sediments are dominated by sands. Because of the energetic currents, accumulation of fine-grained sediments is mostly confined in a mud depocenter southeast of the Helgoland Island, that is the HMA (Figure 1c).

The HMA extends over 500 km^2 with a mean water depth of ∼20 m. It is located on a slope between the water depth of 15 and 35 m, bridging the shallow water (the outer Elbe River estuary) and the deeper bathymetric depression, which is part of the paleo-Elbe Valley. Up to 30 m thickness of sediments have accumulated in the HMA since the mid-Holocene (∼6,000 cal. yr BP, von Haugwitz et al., 1988). There exists a spatial heterogeneity of sediment composition in the HMA, with finer (clay and silt) sediments in the southwestern part and coarser (silt and fine sand) sediments toward the northeastern part (Hebbeln et al., 2003, see also Figure 1c). The sedimentation rates in the HMA during the past 6,000 years are estimated to range between 2 and 20 mm yr^{-1}. A marked drop of the sedimentation rate from >13 to ∼1.6 mm yr^{-1} at around 1,250 A.D. has been identified. Since then, the rates have become stable over the last 750 years (Hebbeln et al., 2003).

2.2. Numerical Model

This study applies a hydro-morphodynamic model, which comprises two major parts: the Semi-implicit Cross-scale Hydroscience Integrated System Model (SCHISM; Y. J. Zhang et al., 2016) for hydrodynamics and the sediment transport and morphodynamics model (MORSELFE; Pinto et al., 2012), which is integrated into SCHISM.

SCHISM is a three-dimensional numerical modeling system, which can address a wide range of physical and biological processes (Y. J. Zhang et al., 2016). The hydrodynamic core employs a semi-implicit advection scheme avoiding the Courant-Friedrich-Lewy condition (CFL) stability constraints (Courant et al., 1928), and can apply to regions with strong bathymetric gradients, such as estuaries, coastal waters, and shelf seas. The combination of unstructured mixed triangular/quadrangular grid in the horizontal dimension and the hybrid (partially Sigma and partially Z, SZ) coordinates or the Localized Sigma Coordinates (Song & Haidvogel, 1994) with Shaved Cell (LSC^2) in the vertical dimension enables a seamless cross-scale simulation of three-dimensional baroclinic circulation. The robust transport schemes are also crucial for the simulation of baroclinic circulation and mesoscale dynamics in cross-scale applications (Ye et al., 2019). The model also incorporates a wetting and a drying scheme in shallow water such as intertidal areas.

The sediment transport and morphodynamics module MORSELFE (Pinto et al., 2012) is based on the community sediment transport model (CSTM; Warner et al., 2008). MORSELFE combines an advection-diffusion model for suspended load transport, empirical formula for bed load transport, and a bed level updating scheme. Classes of suspended sediment are represented by tracer concentration values with sinking velocities dependent on

Table 1
Configuration of Sediment Classes in the Model

Sediment class	Settling velocity (mm/s)	Erosion rate constant (s/m)	Critical shear stress for erosion (Pa)
Clay	0.001	1×10^{-4}	0.2
Medium silt	0.1	1×10^{-4}	0.1
Coarse silt	0.4	1×10^{-4}	0.067
Fine sand	0.8	2×10^{-4}	1.0

Note. Erosion rate formulation is set according to Winterwerp et al. (2012).

the grain size. The sediment module is two-way coupled to the hydrodynamic module to resolve the hydro-morphodynamics.

2.3. Model Setup for the Study Area

The model domain spans from 40° N to 66°N in latitude and 20°W to 30°E in longitude (Figure 1a), covering the North Atlantic including the North Sea and the Baltic Sea with two open boundaries: the boundary at north of North Sea and the boundary at south—west of North Sea. The hydrodynamic setup is based on previous studies by Kossack et al. (2023) and Porz et al. (2024), which have been validated for the North Sea. In this study, the overall model setup including forcing data is comparable to their setup but with a refinement in grid resolution in the German Bight, which has been made to better resolve the nearshore processes. Around the HMA, the spatial grid resolution is ∼700 m. The horizontal grid comprises a total number of ∼89 k grid nodes and ∼169 k triangular grid elements. Bathymetry is interpolated from the 50 × 50 m resolution data provided by the European Marine Observation and Data Network (EMODnet). The LSC^2 coordinate is used in the vertical dimension to resolve the near-bottom dynamics. In terms of vertical resolution for resolving baroclinic forcing, 52 layers are configured for deep water (e.g., the continental slope and the basin), which gradually decrease to 10–12 layers in the HMA and adjacent shallow water. The hourly atmospheric forcing is provided by the atmospheric hindcast simulation coastDat-3 (Helmholtz-Zentrum Geesthacht, 2017). The initial fields of temperature and salinity are derived from the World Ocean Atlas 2018 (WOA2018) climatological data (Boyer et al., 2018; Locarnini et al., 2019; Zweng et al., 2019). Hourly time series of surface water level and currents from the HYbrid Coordinate Ocean Model (HYCOM) derived from Samuelsen et al. (2022) are specified at the open boundary, which is additionally forced by tides from the FES2014 (Lyard et al., 2021) using 15 tidal constituents (Q1, O1, P1, S1, K1, 2N2, MU2, N2, NU2, M2, L2, T2, S2, K2, and M4) that constitute more than 99% of total tidal energy in the offshore region. Higher order tidal constituents such as M8, M6, and MS4 are generated by interaction between the primary tides (e.g., M2 and S2) and shallow water zones in the model domain (Figure S1 in Supporting Information S1). Daily discharge rates of river runoff and sediment are specified for the major rivers in the North Sea including the River Elbe (Kossack et al., 2023, see also Figure S2 in Supporting Information S1).

In our simulation, the surface seabed sediment configuration follows that of Porz et al. (2024) but with a higher grid resolution in the German Bight. Four sediment classes, namely clay, medium silt, coarse silt, and fine sand, are specified for the initial seabed with respective fractions defined according to Bockelmann et al. (2018) (Table 1). Two additional classes, namely riverine clay and riverine medium silt are additionally introduced at the river boundary. The purpose of distinguishing the riverine sediment with the existing seabed sediments is to trace the transport of each class individually so that their relative contribution to the deposition in the HMA area can be quantified. The initial erodible seabed surface sediment was divided into 30 vertical layers, each with an initial thickness of 1 cm. During simulation, the erodible sediment layer thickness and fractions of each sediment class in these layers are dynamically adjusted based on erosion and deposition. A constant concentration of 40 mg L^{-1} for discharged sediment is specified at the river boundaries according to the median value derived from nine major rivers in the southern North Sea by Abril et al. (2002). The impact of flocculation on the settling velocity is negligible due to a persistently low suspended sediment concentration (<100 mg L^{-1}) in the study area. Despite ∼1.2×10^6 m^3 and ∼2.7×10^6 m^3 of dredged sediment dumped in the study area in 2013 and 2014, respectively (Hafen & Nach Neßsand, 2013, 2014), this was not included in our modeling since we focused mainly on the physical mechanisms of sediment accumulation. Potential anthropogenic influence including dumping is discussed in Section 4.

Table 2
Data Sources Used for Model Initialization (Init.), Forcing (Forc.), Parameterization (Param.), and Model Validation (Valid.)

Data type	Use	Time	Description	Source/provider
Hydrodynamics: atmospheric forcing	Forc.	1979–2017	coastDat-3: atmospheric hourly hindcast for Western Europe and the North Atlantic using COSMO-CLM version 5.00_clm8	Helmholtz-Zentrum Geesthacht (2017)
Hydrodynamics: climatological data	Init. and Forc.	1955–2017	WOA2018: climatological fields of in situ temperature and salinity	Boyer et al. (2018)
Hydrodynamics: oceanic forcing	Forc.	1948–2014	HYCOM-ECOSMO: open boundary conditions hindcast simulation of the North Atlantic: daily averaged subtidal SSH and horizontal velocities	Samuelsen et al. (2022)
Hydrodynamics: tides	Init. and Forc.	2012–2014	FES2014: finite-element global ocean tide atlas	Lyard et al. (2021)
Hydrodynamics: river discharge	Forc.	1986–2015	Daily river forcing for the 172 largest rivers computed from a regional river data set	Zhao et al. (2019)
Hydrodynamics: river discharge	Forc.	2000–2022	Data from FGG Elbe: daily river forcing for the Elbe River	Flussgebietsgemeinschaft Elbe/Elbe River-basin association (FGG Elbe, 2024)
Hydrodynamics: water level	Valid.	2014	CMEMS AMM15: observation data at the tide gauge stations: Helgoland, Norderney, Hoernum and Alter Weser	Tonani et al. (2019); Wasserstraße und Schifffahrtsverwaltung des Bundes (WSV, 2023)
Hydrodynamics	Valid.	2014	Operational model data (Circulation model BSHcmod) includes water level, currents, temperature, salinity	Dick et al. (2020)
Sediment	Param.	–	Mud content and median grain size of North Sea sediments	Bockelmann et al. (2018)
Sediment	Param.	1996–2016	EasyGSH-DB: sediment D50	Sievers et al. (2020)
Observation	Valid. and Param.	2022	Cruise data from RV Heincke HE595: lander stations, CTD and ADCP	Tippenhauer, S. (2022)

The model first simulated for 1 year as spin-up based on the initial setting and realistic forcing in 2012, and then continued to simulate the year 2013 and 2014. The results for 2013 and 2014 were analyzed in our study. The reason for choosing 2013 and 2014 was because these 2 years are featured by high (maximum exceeding 4,000 $m^3 s^{-1}$ in 2013) and low (maximum around 800 $m^3 s^{-1}$ in 2014) river discharge (Figure S2 in Supporting Information S1), representing distinct impacts of rivers in terms of freshwater plume and sediment discharge.

2.4. Observation Data

Observation data constitute an important resource for the parameterization, initialization, calibration, and validation of the model. In addition to existing open-source data, field observations from a cruise HE595 in 2022 in the HMA were also used for qualitative assessment of our simulation results. A full list of observation data as well as the purpose of these data for our study are provided in Table 2.

2.5. Identification of Fronts

In the German Bight, two types of density fronts exist, including the salinity front associated with freshwater discharge from the rivers and the tidal mixing front associated with tidal mixing and stratification caused by the temperature gradient. They play a critical role in controlling sediment transport and deposition (Ricker et al., 2021).

To identify the bottom salinity front, we calculated the horizontal gradient of bottom salinity over the entire region based on the simulation results. We identified the salinity front by the largest gradient (VS), which is calculated by

$$\nabla S = \frac{\partial S}{\partial x}\hat{i} + \frac{\partial S}{\partial y}\hat{j}, \tag{1}$$

where S is the bottom salinity, x and y are the horizontal coordinates, and i and j are the unit vectors on x and y directions, respectively.

To evaluate the spatial heterogeneity of the vertical salinity gradient over the model domain, we also calculated the horizontal gradient of the maximum vertical salinity gradient for each grid cell by

$$\nabla S_{v\max} = \frac{\partial S_{v\max}}{\partial x}\hat{i} + \frac{\partial S_{v\max}}{\partial y}\hat{j}, \tag{2}$$

where $S_{v\max} = \max\left(\frac{\partial S}{\partial z}\right)$ refers to the maximum vertical salinity gradient at each local grid cell and z is the vertical coordinate. The physical interpretation of Equation 2 pertains to variations in the strength of the halocline. A larger value indicates more rapid changes in the salinity-induced stratification, which also aids in identifying the boundary between freshwater-induced stratified and well-mixed water.

Various methods have been proposed to identify the tidal mixing fronts. We adopted three different approaches from existing literature to compare their results for analysis. The simplest measure of thermal stratification is to calculate the difference between the sea surface temperature (SST) and the sea bottom temperature (SBT) as follows:

$$\Delta T = SST - SBT, \tag{3}$$

Tidal mixing fronts in the shallow water region between 50 and 100 m form when tidal mixing balances buoyancy production due to incoming solar radiation (Simpson & Hunter, 1974). In a study conducted by Timko et al. (2019), it was found that there is a high correlation between the location of the mixing front defined in terms of the sea surface to seabed temperature difference ($\Delta T = 0.5°C$) and the location defined in terms of the potential energy anomaly in the northeast Atlantic shelf. In the simplest measure, we also adopted the $\Delta T = 0.5°C$ to identify the mixing front. Another method we adopted is based on the horizontal gradient of the maximum vertical temperature gradient (similar to Equation 2):

$$\nabla T_{v\max} = \frac{\partial T_{v\max}}{\partial x}\hat{i} + \frac{\partial T_{v\max}}{\partial y}\hat{j}, \tag{4}$$

In addition, we also calculated the Simpson-Hunter parameter (Sh; Glorioso & Simpson, 1994), which is often used to predict the location of tidal mixing fronts for constant heat flux as follows:

$$S_h = \log 10\left(hu^{-3}\right), \tag{5}$$

where h is the local water depth, and u is the depth averaged current velocity. In a numerical modeling study by Holt and Umlauf (2008), $Sh = 3.0 \pm 0.3$ was found to correspond to the mean frontal position based on model comparison with ~80,000 ΔT observation values provided by the International Council for the Exploration of the Sea (ICES Dataset on Ocean Hydrography, 2014; http://geo.ices.dk). We adopted the same critical value ($Sh = 3.0 \pm 0.3$) to identify the location of the tidal mixing fronts. Results from all three abovementioned methods are compared and analyzed.

3. Result

3.1. Model Validation

The hydrodynamic model has been validated by Kossack et al. (2023). We have further assessed the model performance in the nearshore area by comparing simulation results of water level, currents, salinity, temperature, and sediment concentration with observation data.

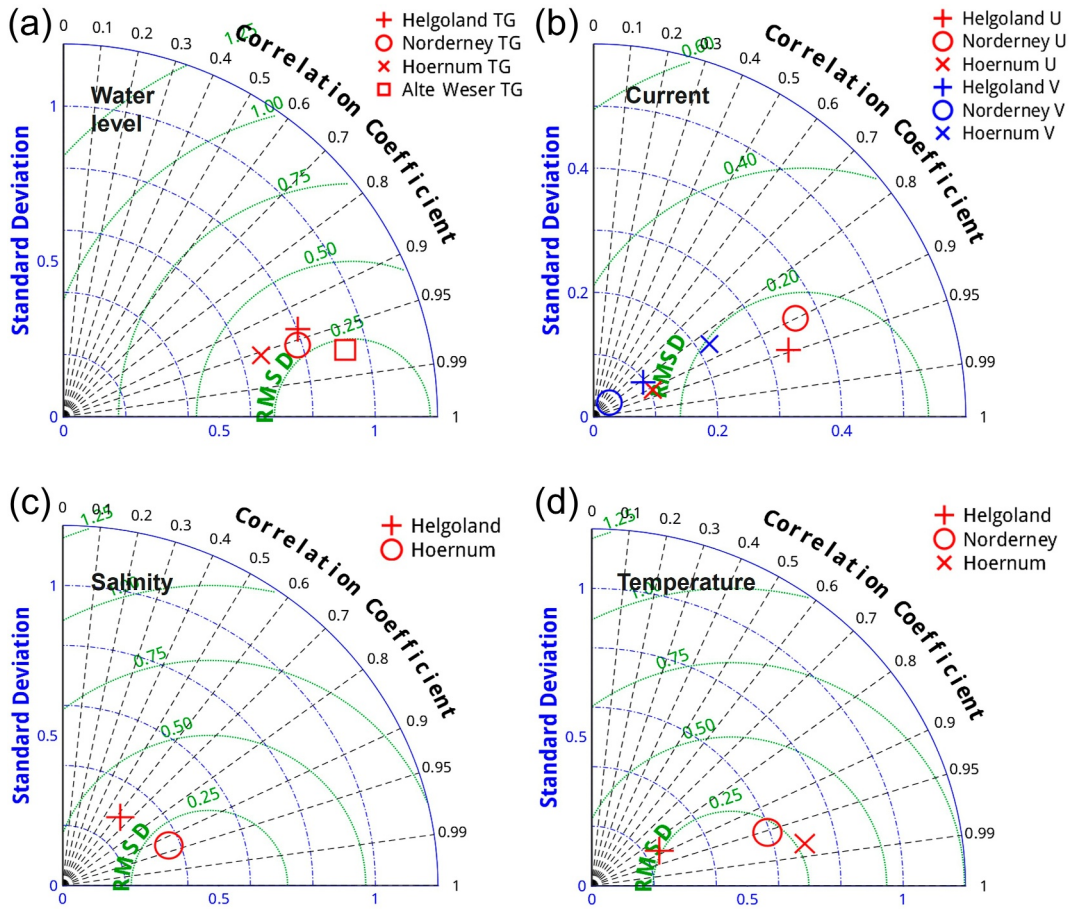

Figure 2. (a) Taylor diagram showing the standard deviation, the correlation coefficient, and the RMSE of simulated water level against field data at the tide gauge stations of Helgoland, Norderney, Hoernum, and Alter Weser in March 2014 as an example to assess the model performance. The radial distance from the origin represents the standard deviation, indicating the variability of the modeled and observed data. The angular position represents the correlation coefficient (r), measuring the strength and direction of the linear relationship between the model and observations, with $r = 1$ indicating perfect correlation. The distance from the observation point on the *x*-axis (reference point) represents the root mean square difference (RMSD), quantifying the overall difference between the model and observations. Comparison between our simulated results with the BSH real-time operational model results at the sites of Helgoland, Norderney, and Hoernum in March 2014. (b) Current of U component (east-west in red) and V components (north-south in blue) (d) temperature. (c) Comparison of salinity at the location of Helgoland and Hoernum in summer of 2014.

3.1.1. Validation of Hydrodynamics

Results indicate that the model performs well on reproducing the hydrodynamics in the German Bight. The comparison between simulated time series (water level, currents, temperature, and salinity) and measurement at the tide gauge stations in Helgoland, Norderney, Hoernum, and Alter Weser (locations in Figure 1a) demonstrates a general satisfactory model performance (Figure 2). For instance, the mean tidal amplitude at the tide gauge station of Helgoland is ∼3.73 m and the root mean square error (RMSE) of the simulated water level is ∼0.33 m, corresponding to 8.8% of the mean amplitude. The correlation coefficient is around 0.95. The assimilated BSH operational model indicates an east-west current component of ∼1.12 m/s at the tide gauge station of Helgoland, and the RMSE of our simulated current is ∼0.11 m/s, corresponding to 9.8% of the reference value (Figure 2a). The correlation coefficient is around 0.9 at the locations of Helgoland, Norderney, and Hoernum. The mean salinity at the station of Helgoland is ∼32 PSU, and the RMSE of simulated salinity is ∼0.36 PSU (Figure 2c). The stations in Norderney and Hoernum are close to the shore and dominated by well-mixed water. The correlation coefficient is a bit higher than that at the Helgoland site with the value of ∼0.95. The correlation coefficient of temperature in March 2014 is higher than 0.95 at the locations of Norderney and Hoernum and ∼0.9 at the location of Helgoland (Figure 2d).

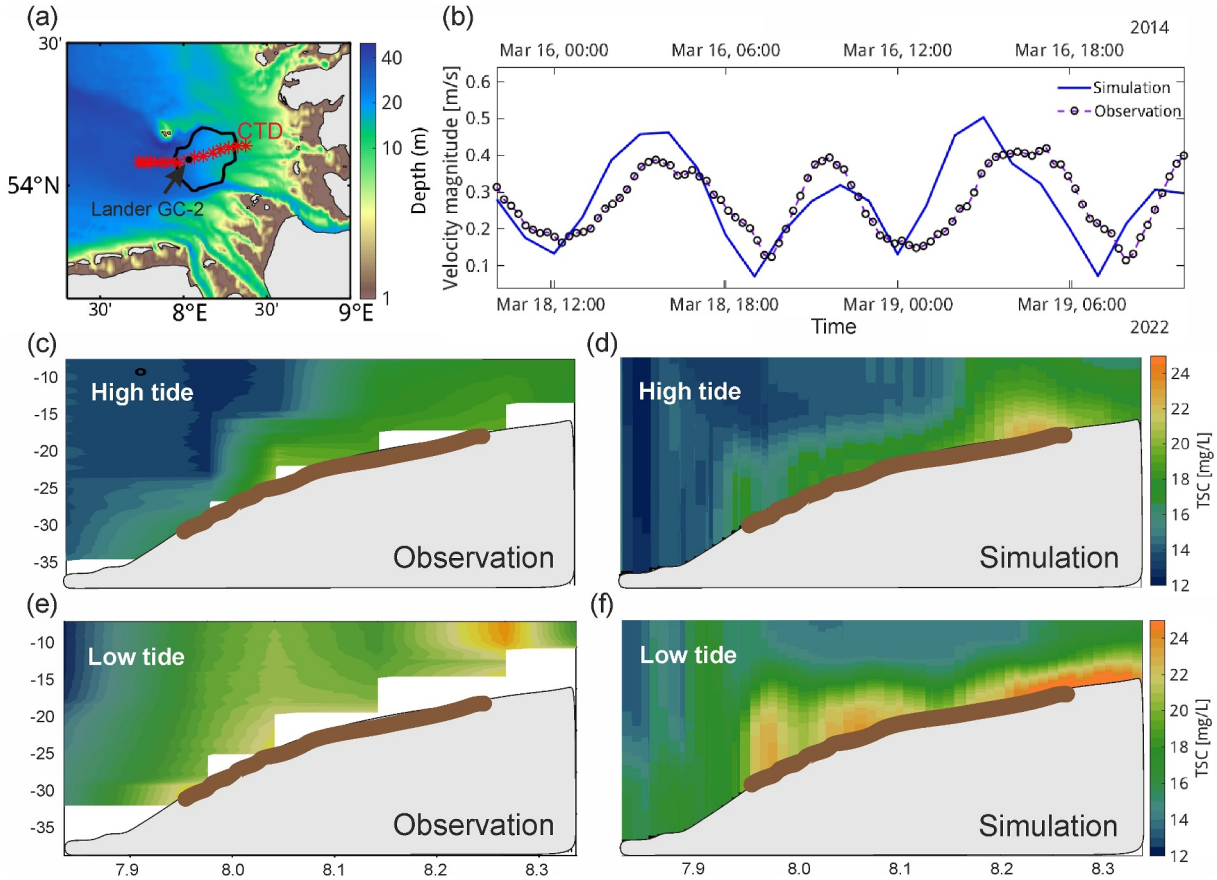

Figure 3. Observations (2022) and model simulation (2014) of bottom current velocity and total suspended particulate matter concentration. (a) Location of the lander station is marked by the black dot and the CTD transect is indicated by the red asterisks. (b) Simulated bottom current velocity magnitude (blue line) and measured value from the lander station (dots). (c) and (e) refer to observation data in the transect in high tide and low tide, respectively. (d) and (f) are snapshots of simulated total SPM concentration in the similar tidal phases. The brown line in (c–f) indicates the location of the HMA.

3.1.2. Validation of Sediment Dynamics

The assessment of simulated total suspended particulate matter (SPM) concentration is done at a qualitative manner due to lack of observation data in the simulated years. The observation in 2022 was implemented in March with relatively calm weather conditions. We selected a similar period in March 2014 characterized by the same spring-neap tidal cycle (Figure 3b) and calm weather conditions for comparison. During this period, the bottom velocity magnitude fluctuates between 0.1 and 0.5 m s^{-1}. The vertical profiles of SPM concentration along the transect show comparable patterns between our simulation and observations. During the high tide, the SPM concentration is higher in the eastern part of the HMA than the western part. During the low tide, two notable high SPM concentrations were observed on the HMA. One is located near the eastern edge, and the other is near the western edge. Similar patterns were also reproduced in our simulation results. The difference is that our simulation results show a stratified structure with high SPM concentration confined near the bottom during the low tide, whereas a more mixed structure was seen in the observation.

3.2. Sediment Accumulation and Bottom Shear Stress

To investigate sediment dynamics during the period of 2013–2014, the net sediment flux across the sediment-water interface and bottom shear stress in the German Bight are assessed based on the simulation results to understand their spatial distribution pattern and heterogeneity. Our elucidation is mainly focused on the winter and summer seasons since they represent distinct and contrasting hydrographic conditions. In winter, the temperature gradient is minimum and sediment dynamics in our study area are mainly affected by the salinity front. By contrast, summer is featured by the strongest tidal mixing front associated with temperature gradient. Spring

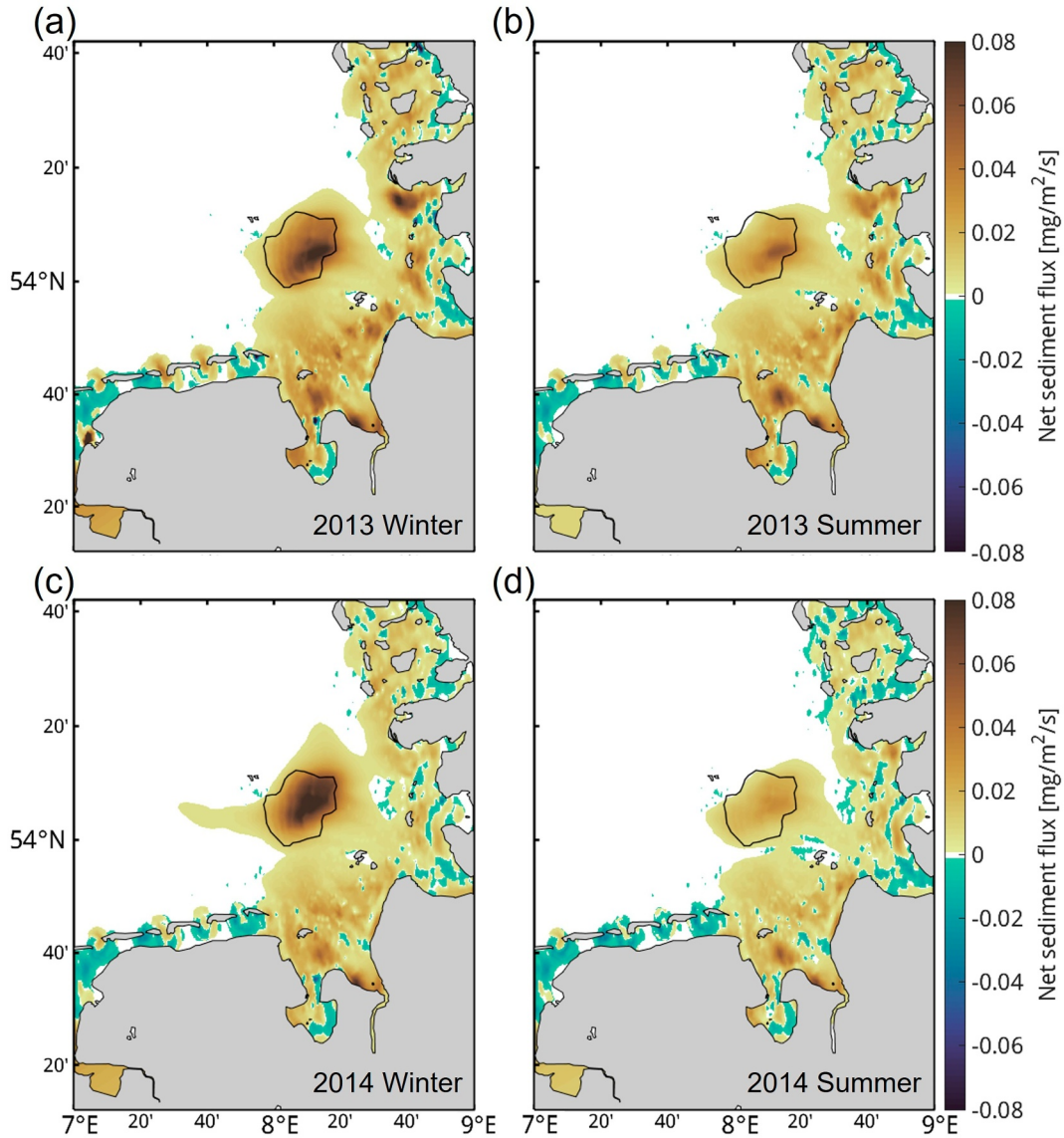

Figure 4. Net vertical sediment flux across the sediment-water interface during the winter and summer periods in 2013 and 2014 derived from simulation. (a) Winter 2013 from December 2012 to February 2013, (b) summer 2013 from June 2013 to August 2013, (c) winter 2014 from December 2013 to February 2014, and (d) summer 2014 from June 2014 to August 2014. Positive and negative values indicate net deposition and erosion, respectively.

and autumn, on the other hand, are transitional periods during which the frontal systems are more variable and exhibit a mixture of winter and summer patterns. For this reason, a comparison between winter and summer provides a clear distinction between the mechanisms of sediment accumulation associated with the two frontal systems (salinity front and tidal mixing front).

The simulation result indicates significant sediment accumulation in the HMA and a vast part of the Wadden Sea areas in both winter and summer seasons (Figure 4). The spatial distribution pattern of net sediment flux across the sediment-water interface is relatively stable over the seasons but characterized by a notable difference in the magnitude. A persistent accumulation in the HMA is seen in the results, albeit with seasonal and spatial variation in the rate. The nucleus area of sediment accumulation in the HMA varies between 2013 and 2014, with maximum deposition in the southeastern part of the HMA in 2013 and shifted to the northeastern part in 2014. In the HMA, winter seasons are featured by a larger sediment accumulation rate than in summer seasons. The net sediment accumulation rate in the HMA in winter 2013 is 88% larger than that in summer 2013. The net sediment

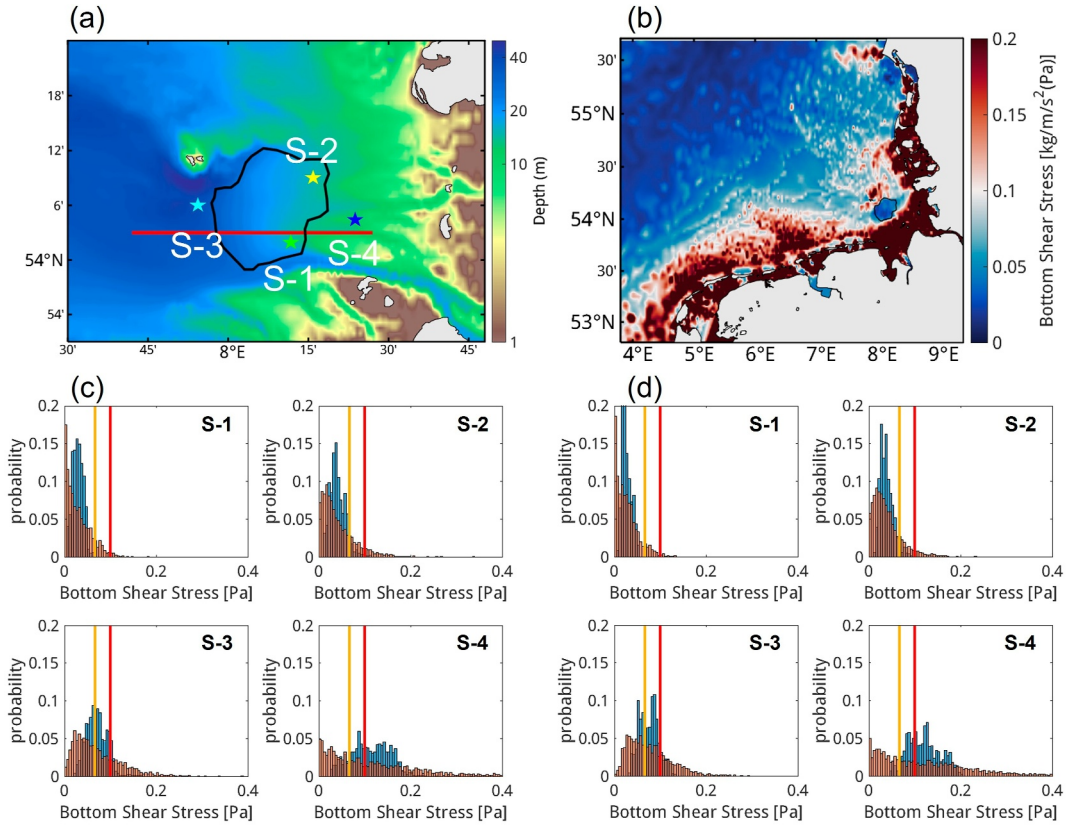

Figure 5. Distribution of simulated bottom shear stress. The stars in (a) indicate the sites selected for analysis: S-1 in the southern part of the HMA, S-2 in the northern part of the HMA, S-3 in the Helgoland Hole on the seaward side of the HMA, and S-4 in shallow water on the shoreward side of the HMA. (b) Simulated annual mean bottom shear stress in 2013. The histograms show the distribution of bottom shear stress, respectively, in (c) winter and (d) summer of 2013 (original shear stress distribution in orange and low-pass filtered shear stress with tidal signals removed in blue). Critical shear stress for resuspension of unconsolidated coarse silt (0.067 Pa) and medium silt (0.1 Pa) are indicated by yellow and red lines, respectively.

accumulation in the HMA in winter 2013 and summer 2013 accounts for ∼32 % and 17 %, respectively, of the total annual net accumulation. It is worth noting that the winter 2014 is featured by most favorable conditions for sediment accumulation in the HMA, with its net accumulation rate accounting for ∼42 % of the total annual accumulation of 2014, despite that the total annual accumulation in the HMA in 2014 is ∼11% lower than that in 2013 (Figure S3 in Supporting Information S1).

Sediment deposition is strongly associated with the bottom shear stress. The spatial distribution of bottom shear stress averaged over the 2 years indicates strong bottom currents along the coasts with exception in the HMA, where the mean bottom shear stress is below the critical shear stress for resuspension of silts (Figure 5). Time series of bottom shear stress at four sites (indicated by stars in Figure 5a) were analyzed to understand the spatial heterogeneity in the HMA area and its surroundings. Results indicate that the bottom shear stress at each site remains relatively stable over the different seasons (Figures 5c and 5d). The shoreward side of HMA (S-4) is characterized by notably stronger bottom shear stress than other sites. The maximum bottom shear stress at S-4 can reach to more than 0.56 Pa. On the other hand, minor difference is seen among the sites within the HMA (S-1 and S-2). Seasonal difference at each site is seen when the tidal signal is removed. In two sites, namely S-1 (southern part of HMA) and S-2 (northern part of HMA), winter season is featured by stronger bottom currents leading to higher bottom shear stress. On the contrary, S-3 (seaward site of HMA) and S-4 (shoreward side of HMA) are characterized by slightly higher bottom shear stress in summer season than in winter season. In the HMA (S-1 and S-2), the duration of bottom shear stress above the threshold for resuspension of fine-grained sediment (0.1 Pa for unconsolidated medium silt) takes up less than 10% of the total time, whereas at S-3 and S-4, the bottom shear stress exceeds 0.1 Pa in more than 30% of the total time. It is worth noting that there exists

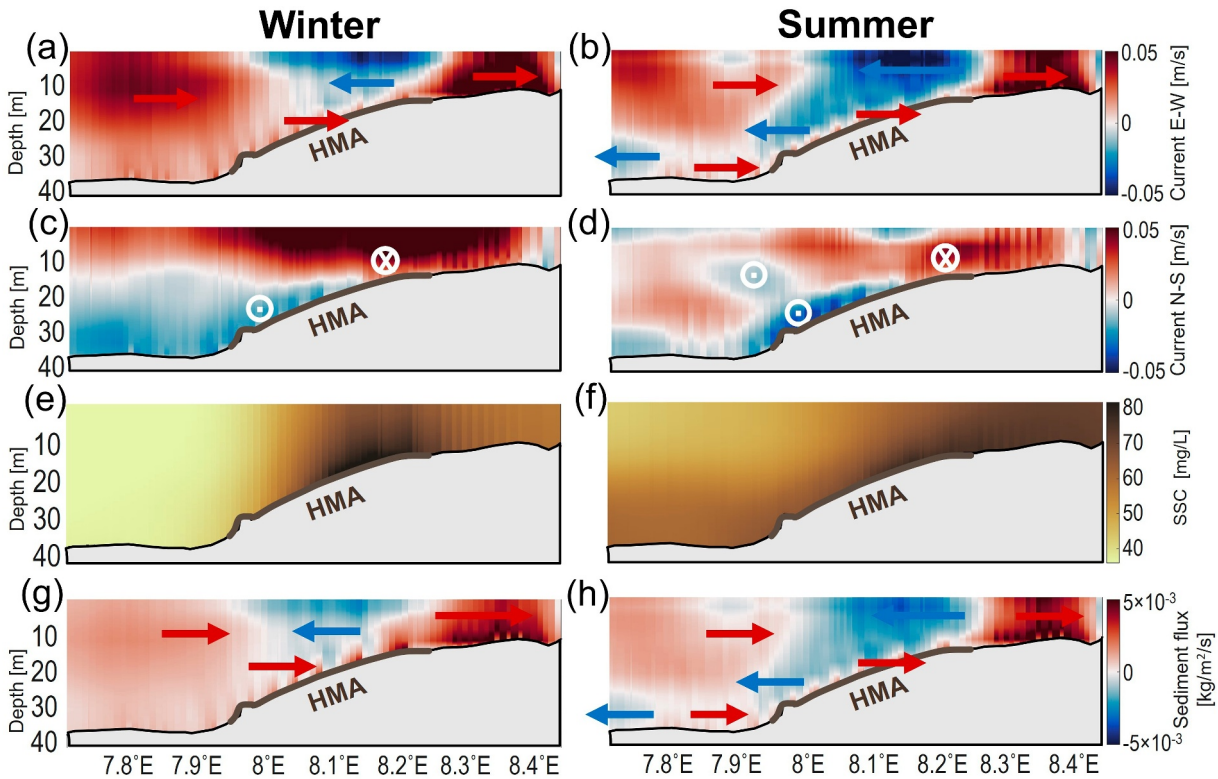

Figure 6. Seasonal-averaged residual current (east-west component) along the transect above the HMA in 2013 derived from simulation. (a) Winter from December 2012 to February 2013. (b) Summer from June 2013 to August 2013. (c) and (d) are the north-south velocity components in the same periods as (a) and (b), respectively. (e) and (f) indicate time-averaged SPM concentration along the transect for the same periods. (g) and (h) refer to the residual sediment flux along the transect (east-west direction).

spatial heterogeneity of bottom shear stress within the HMA as shown by the difference between S-1 and S-2. At S-1, the period below the threshold of resuspension of coarse silts (0.067 Pa, representing the most vulnerable sediment class to resuspension) persists by 10% longer than that at S2, providing more favorable condition for settling and consolidation of fine-grained sediment.

3.3. Residual Current and Sediment Transport

Seasonal-averaged residual current and sediment transport flux derived from the simulation provide further information on the net transport direction and magnitude of SPM and its relationship with the HMA. Along the transect (east-west direction) across the HMA, the residual current shows an onshore transport in the bottommost water layer and offshore transport above this layer (Figures 6a and 6b). Meanwhile, the residual current is directed northward on the shallow part of the HMA and southward on the deep part of the HMA (Figures 6c and 6d). Such a residual current pattern is quite stable and exhibits only minor variations between summer and winter. Spring and autumn are transitional phases between winter and summer and exhibit similar patterns. Time-averaged SPM concentration shows a higher level above the HMA than its adjacent offshore and onshore areas during winter (Figure 6e). In summer, the SPM concentration is reduced above the HMA compared to winter, while is notably increased in its adjacent offshore and onshore areas (Figure 6f). Residual sediment transport is closely linked to the residual currents (Figures 6g and 6h). The magnitude of residual sediment transport flux is higher in the bottom water than in middle or surface water, suggesting a dominant control of SPM transport by bottom currents. The shoreward directed transport in the bottom water and seaward-directed transport above the bottom water provides a trapping mechanism for SPM on the HMA.

A horizontal view of the residual current and sediment transport directions also confirms their general consistency with only slight differences. Results of the residual sediment transport indicate opposite transport patterns between the surface and bottom water layers in the study area (Figure 7). In winter, surface residual sediment

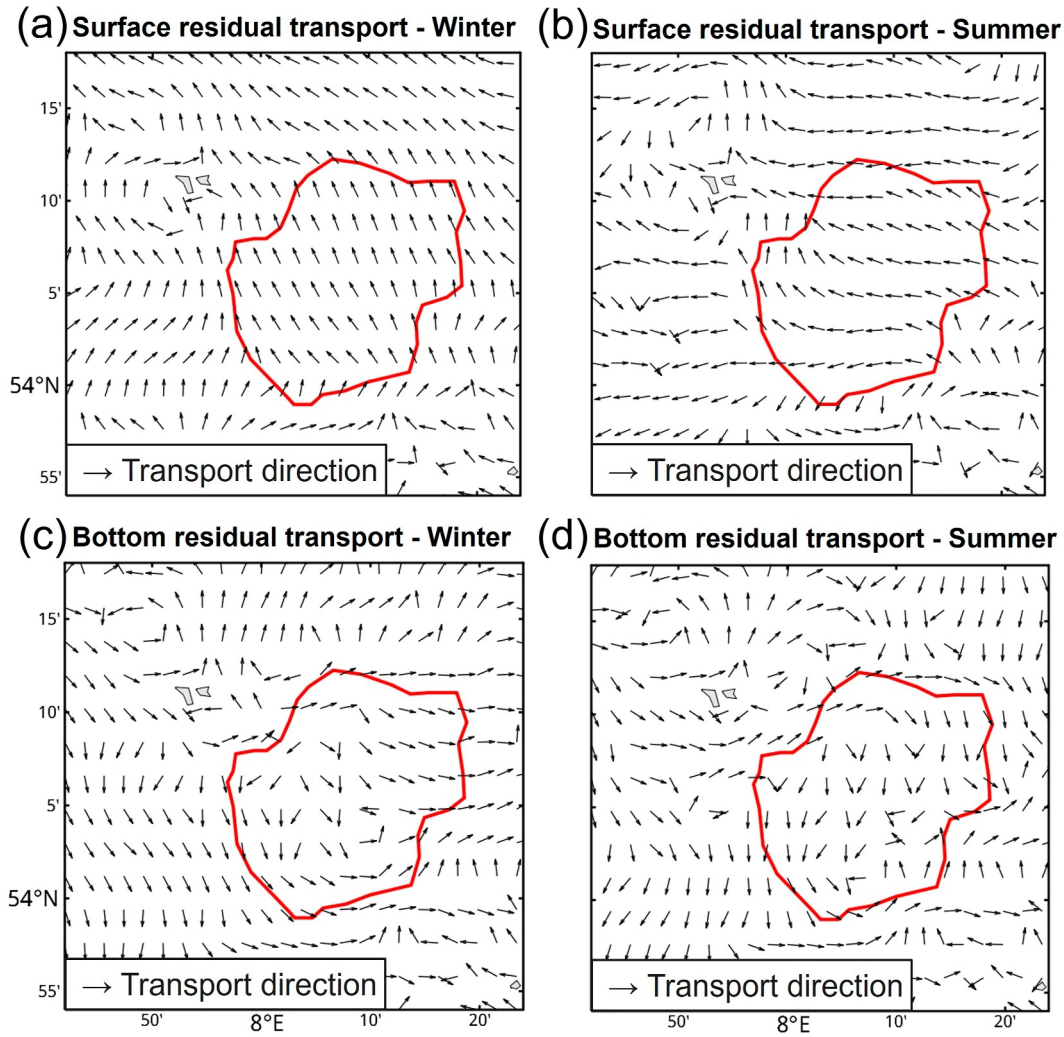

Figure 7. Surface and bottom residual sediment transport direction derived from simulation. (a) and (c) are for winter from December 2012 to February 2013. (b) and (d) are for summer from June 2013 to August 2013.

transport is directed northward in the HMA and adjacent areas, whereas the bottom residual sediment transport is directed southward in the western side of the HMA and gradually shifted northward in the eastern side of the HMA. It is worth noting that the transition of the bottom sediment transport direction occurs in the HMA, forming a vortex-like circular motion, which facilitates accumulation of SPM in its center. In summer, surface sediment transport in the HMA is mainly directed westward in its southern part and northwestward in its northern part. By contrast, a dominant southward transport is seen in the bottom water in the HMA. It is particularly worth noting that convergence of bottom residual sediment transport is seen in various parts of the HMA in both winter and summer periods. Because most SPM is transported in the bottom water layers (Figure 6), a depth-integrated transport (Figure 8a) indicates a net sediment transport from the paleo-Elbe Valley and the southwestern coasts toward the HMA, suggesting these areas as potential sediment sources of HMA. By contrast, only a small portion of residual sediment transport from the Elbe River mouth is directed toward the HMA in the surface water (Figure 7) and the depth-integrated residual sediment transport indicates a net transport into the Elbe River (Figure 8a).

Calculation of the accumulative sediment transport flux across the four boundaries of the HMA in the period of 2013–2014 (Figure 8b) indicates that the western and southern boundaries are mainly featured by sediment input, with the total mass of inflow larger than the outflow. By contrast, the eastern and northern boundaries are mainly featured by sediment output. This is consistent with the transport pathways illustrated in Figure 8a. The results

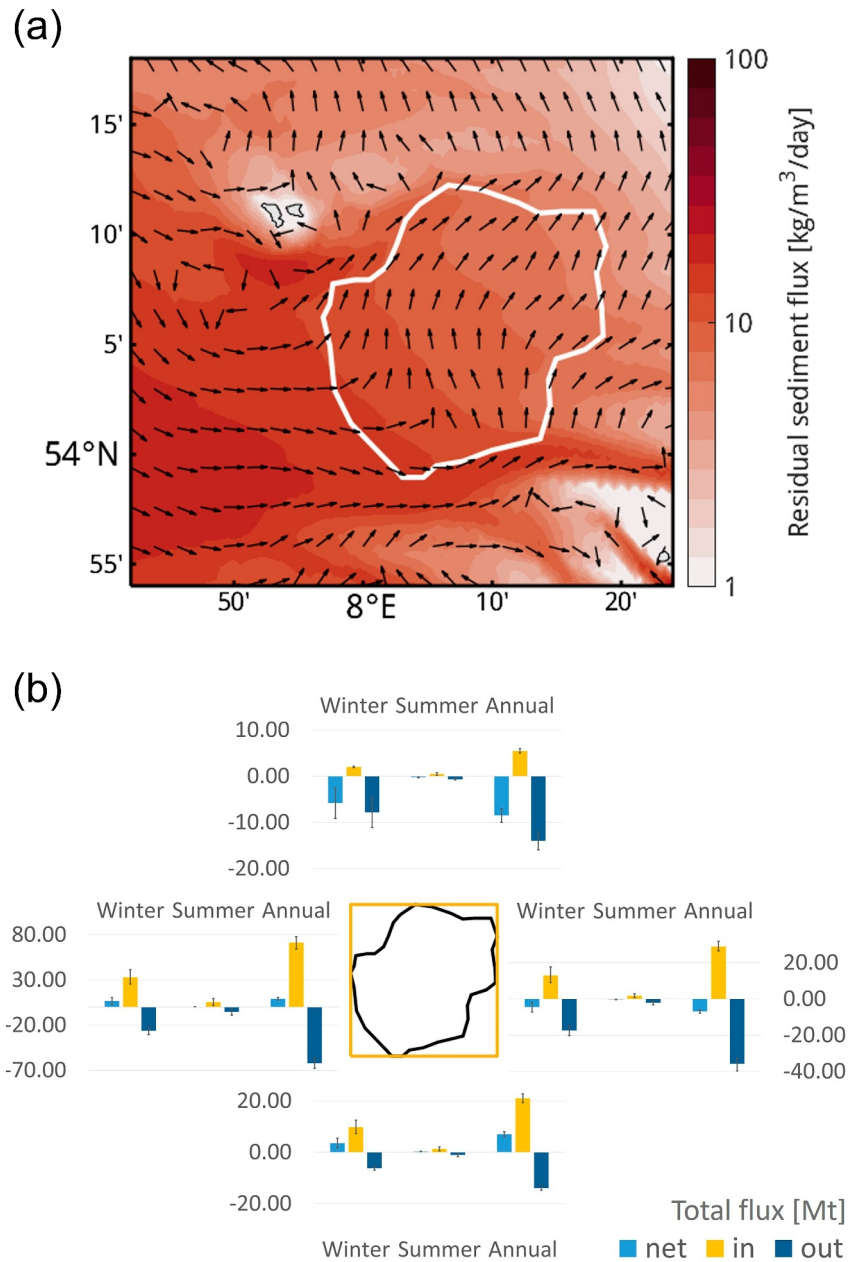

Figure 8. Depth-integrated residual sediment transport pattern and budget analysis for the HMA area derived from simulation. (a) Annual mean residual sediment transport flux for 2013–2014. Transport direction is indicated by arrows, and magnitude is represented by color. (b) Accumulative amount of sediment transport across the four open boundaries of the HMA for winter, summer, and the entire year of 2013 and 2014. The value range is indicated by the error bars. Positive and negative values refer to inflow to and outflow from the HMA, respectively.

also indicate that sediment transport across the boundaries is much more active in winter than in summer, and the exists a discrepancy between the total sediment input and output, indicating that ~0.8 Mt (~0.65 Mt in 2013 and ~1.04 Mt in 2014) of inputted sediment is deposited in the HMA annually.

3.4. Stratification and Frontal System

To further investigate the physical mechanisms of sediment trapping and deposition on the HMA, we assess the role of the frontal systems associated with salinity and temperature gradient.

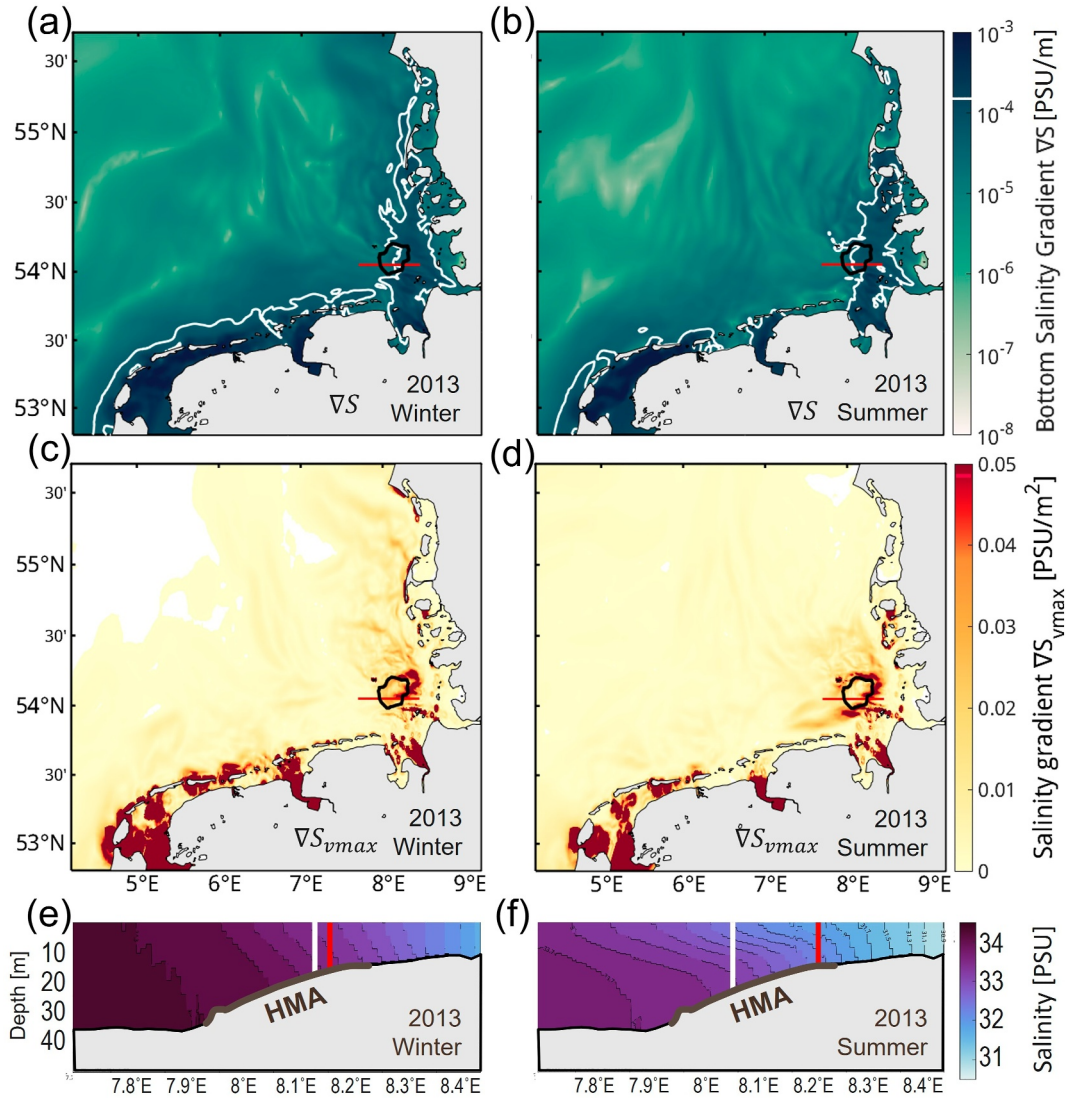

Figure 9. Location of the salinity fronts in the German Bight in 2013 inferred from simulation. (a and b) Bottom salinity gradient ∇S averaged in winter and summer, respectively. The maximum value is indicated by the white contour line. (c) and (d) are the horizontal gradients of the maximum vertical salinity gradient ∇S_{vmax}. (e) and (f) Vertical distribution of salinity along the transect crossing the HMA averaged in winter and summer, respectively. White and red lines indicate the location of the maximum ∇S and ∇S_{vmax}, respectively.

3.4.1. Salinity Fronts

Location of the bottom salinity front is indicated by the maximum value of the bottom salinity gradient ∇S (Figures 9a and 9b). Results suggest that the salinity front is persistently located above the HMA with minor seasonal fluctuations. In the winter of 2013, the front is located close to the shoreward edge of the HMA, while it migrates offshore toward the seaward edge of the HMA in the summer of 2013 induced by a remarkable increase of freshwater discharge from the Elbe River associated with a river flood. Large values of the horizontal gradient of the maximum vertical salinity gradient ∇S_{vmax} are persistently located at the shoreward edge of the HMA in both seasons (Figures 9c and 9d), indicating the shoreward part of the HMA and its adjacent area as a stable transition zone between freshwater-induced stratified water and well-mixed water. A comparison between 2013 and 2014 indicates a relatively stable spatial distribution of ∇S and ∇S_{vmax}, with small differences in summer induced by a difference in the river discharge.

3.4.2. Tidal Mixing Fronts

Tidal mixing fronts are strongest in summer due to greatly enhanced solar radiation, while their impact is minimum in winter because of a largely reduced vertical gradient of temperature. The locations of the tidal mixing fronts inferred from the surface and the bottom temperature difference $\Delta T = 0.5\ ^{\circ}\mathrm{C}$, the horizontal gradient of the maximum vertical temperature gradient $\nabla T_{v\max}$, and the Simpson-Hunter parameter $\mathrm{Sh} = 3.0$ all suggest that the tidal mixing front persistently crosses the HMA in summer (Figure 10). A comparison between the summer of 2013 and 2014 indicates that the spatial distribution of S_h is the most stable among the three parameters. The contour line of $\Delta\mathrm{T} = 0.5^{\circ}\mathrm{C}$ and the edge of the maximum $\nabla T_{v\max}$ exhibit certain spatial fluctuations above the HMA, mainly driven by a difference in the river discharge between the summer of 2013 and 2014. The abnormally high river discharge in June 2023 associated with the river flood causes a shoreward shift of the contour line of $\Delta\mathrm{T} = 0.5^{\circ}\mathrm{C}$ and the edge of the maximum $\nabla T_{v\max}$ compared to a normal summer condition represented by 2014.

As shown in Figure 9, the salinity front is consistently located above the eastern (shoreward) part of the HMA and results in a classical estuarine-like circulation, whereas the tidal mixing front is located above the western (seaward) part of the HMA in summer and leads to a convergence of onshore-directed current from the seaward side of the HMA and offshore-directed current from the shoreward side of the HMA and a circulation at the front (Figure S4 in Supporting Information S1). These dynamic features of the two frontal systems create a unique mechanism that not only effectively transports SPM from both shoreward and seaward sides of the HMA to the HMA but also traps fine-grained sediment particles in the HMA.

3.5. Drivers of Sediment Deposition

To identify the forcing that promotes deposition of SPM on the HMA, we performed Pearson correlation analysis on a set of variables. One correlation analysis is done between the time series of bottom shear stress and related forcing excluding tides. These include wind and extreme events (river floods and storm surges). The baroclinic forcing related to salinity and temperature gradient is collectively represented by the potential energy anomaly (PEA). The other correlation analysis is done between the time series of net sediment flux across the sediment-water interface and related forcing mentioned above. To exclude the impact of tides, a Butterworth low-pass filter was applied to the time series with the cutoff frequency of 24 hr. Both correlation analyses are calculated for all grid cells over the entire German Bight, producing a spatial distribution of the correlation.

Results show that the net sediment flux across the sediment-water interface is closely related to the bottom shear stress, which exhibits a high negative correlation ($r < -0.5$, with minimum value of -0.61 and $P < 0.01$) with stratification, as measured by the PEA, in the eastern part of HMA and adjacent area (Figure 11a). This indicates that enhanced stratification in the eastern part of HMA, which is mainly caused by the vertical salinity gradient associated with the freshwater plume, leads to lower bottom shear stress that favors sediment deposition there. By contrast, a positive correlation between PEA and bottom shear stress is seen in the western part of HMA, indicating higher bottom shear stress and reduced sediment deposition by enhanced stratification, which is mainly caused by the vertical temperature gradient.

The estuarine circulation, driven largely by freshwater runoff, is particularly prominent during periods of weak wind forcing, such as in summer. This circulation facilitates offshore transport of fresh surface water and compensatory onshore transport of sediment-rich bottom water, particularly along the postglacial Elbe Valley (Hofmeister et al., 2017). However, this seasonal signal is overwritten in winter when stronger wind forcing dominates. To further distinguish the individual impact of thermal and haline stratification, additional correlation analysis was performed for summer only, minimizing the influence of wind forcing (Figure S5 in Supporting Information S1). The results reveal a stronger positive correlation between PEA and bottom shear stress in the western HMA during summer than the annually averaged correlation. The area of positive correlation aligns closely with the zone of high thermal stratification (Figure 10) in summer of 2013, while the haline stratification is confined to the eastern HMA (Figure 9) and accounts for the negative correlation there. The opposite correlation patterns with bottom shear stress between salinity-induced and temperature-induced stratification suggest that although both frontal systems cause a convergence of sediment transport in the HMA, their role in sediment deposition is different.

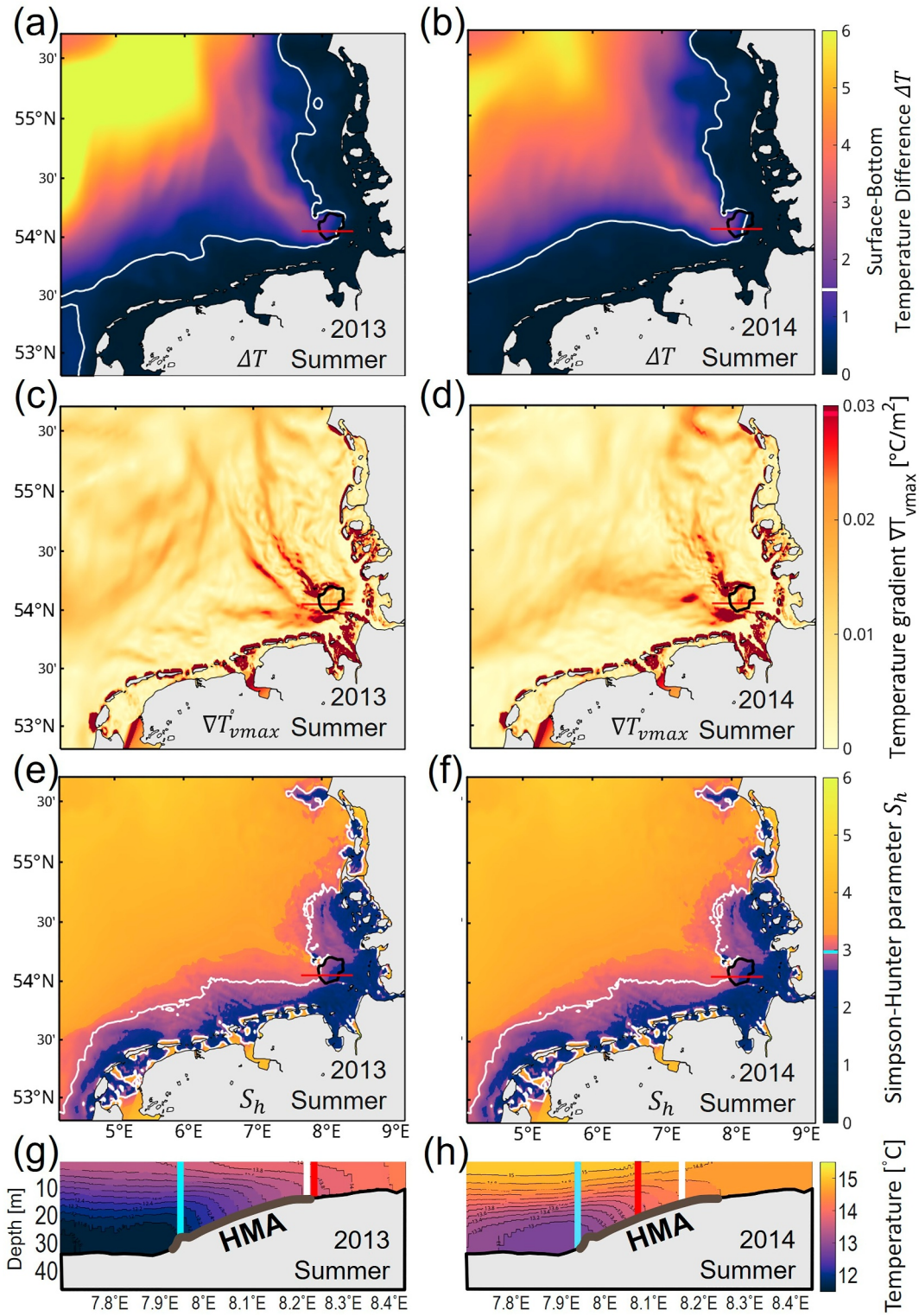

Figure 10. Spatial distribution of the tidal mixing fronts in the German Bight inferred from simulation. (a) and (b) Averaged temperature difference between the surface and the bottom water (ΔT) in summer of 2013 and 2014, respectively. The contour line of $\Delta T = 0.5$°C is marked by white color. (c) and (d) Horizontal gradients of the maximum vertical temperature gradient ∇T_{vmax} for the same periods as (a) and (b). (e) and (f) The calculated Simpson-Hunter parameter S_h for the same periods as (a) and (b). The contour line of Sh = 3.0 is marked in white. (g) and (h) Averaged temperature field along the transect crossing the HMA with the location of $\Delta T = 0.5$ °C (white line), maximum value of ∇T_{vmax} (red line), and Sh = 3.0 (blue line) marked for summer of 2013 and 2014, respectively.

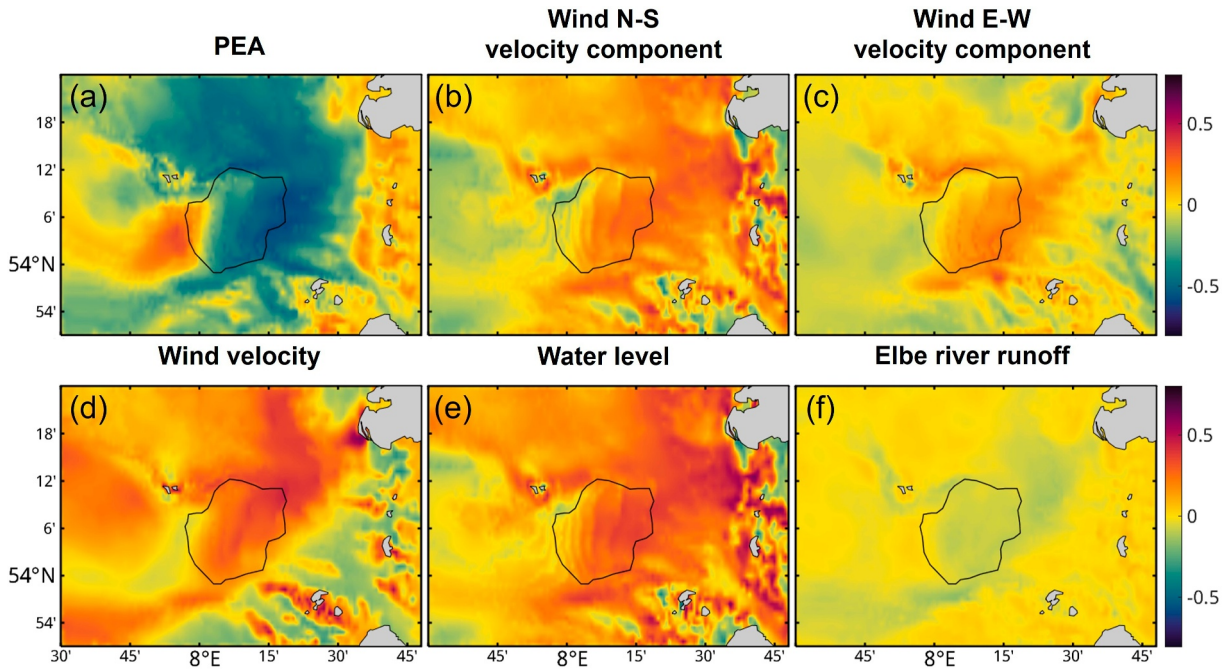

Figure 11. Spatial distribution of the Pearson correlation coefficient (r) between the hourly time series of simulated bottom shear stress and each related forcing in the year of 2013. Positive and negative values in the north-south wind velocity component indicate southerly and northerly wind directions, respectively. Positive and negative values in the east-west wind velocity component indicate westerly and easterly wind directions, respectively. The HMA is outlined by the black polygon.

Other involved forcing also influences bottom shear stress and sediment deposition, but with a weaker correlation than stratification. A positive correlation ($r \leq 0.4$, $P < 0.05$) between wind velocity and bottom shear stress is seen in the HMA, indicating a direct influence of wind strength in sediment deposition on the depocenter. A decomposition of the wind vectors to its north-south and east-west components and their respective correlation with bottom shear stress indicate that the north-south wind component has a slightly stronger influence than the east-west wind component in the HMA (Figures 11b and 11c). An increase of the southerly wind velocity or decrease of the northerly wind velocity leads to a generally larger bottom shear stress. A similar response is seen with an increase of the westerly wind velocity or decrease of the easterly wind velocity. A combined effect of these two correlations indicates that southwesterly winds have the most influential impact on bottom shear stress and sediment deposition in the HMA among all wind directions. This is also reflected in the correlation between bottom shear stress and water level (Figure 11e), since an increase of the latter is largely induced by the southwesterly winds. A weak negative correlation ($r \geq -0.2$, $P < 0.05$) between bottom shear stress in the HMA and the Elbe River runoff is seen, suggesting that the instantaneous runoff of the Elbe River does not have a significant impact on the bottom shear stress and sediment deposition in the HMA. A time lag response may exist due to the distance between the HMA and the river mouth but is of high variability due to the impact of wind, tides, and longshore coastal circulation.

4. Discussion

4.1. Mechanisms of Sediment Trapping and Deposition

Our results show that the joint effect of coastal circulation and the frontal systems acts as an efficient mechanism for delivering fine-grained sediment to the HMA as well as trapping the sediment in the HMA. The resultant residual currents exhibit a distinct seasonal variation that influences the efficiency of sediment trapping in the HMA (Figure 6). Sediment deposition in the HMA is most significant in winter, when an anticlockwise bottom circulation is formed in the southeastern part of the HMA (Figure 7) promoting sediment accumulation and deposition there (Figure 7c). This vortex-like circular motion has also been described by Mayer (1995) as the primary diver of fine-grained sediment deposition in the HMA. However, the depositional area inferred from the result of Mayer (1995) is located directly south of the Helgoland Island in the bathymetric depression, which does

not match the exact location of the HMA that sits more eastward on the slope (Figure 1c). Moreover, there is also a notable mismatch in the maximum deposition area between the results of Mayer (1995) and the field data reported by Hebbeln et al. (2003) and Müller et al. (2024). Our results are able to capture the spatial heterogeneity of sediment deposition in the HMA and indicate that the maximum deposition area is located in the southeastern part of the HMA, which generally fits the field data.

Our results further suggest that although the German Bight is featured by energetic hydrodynamic conditions, the frontal systems especially the salinity front in the HMA remain relatively stable with small fluctuations over the seasons. This enables a persistent sediment convergence and trapping in the HMA. A strong correlation between stratification intensity (represented by PEA), bottom shear stress, and net sediment deposition flux further indicates a critical role of the frontal systems in controlling sediment deposition in the HMA. According to Stanev et al. (2015), vertical stratification enhanced by freshwater inflow reduces erosion in the tidal channels and promotes sediment accumulation in bottom water by limiting vertical sediment exchange between the bottom and surface water layers. This is confirmed by our results. During periods of high river discharge, the salinity front shifts seaward, enhancing stratification and sediment deposition (Zeiler et al., 2014). The nearshore coastal zone of the southern North Sea is remarkably influenced by freshwater runoff, notably from the Rhine and Elbe outflows (Ricker et al., 2021). When the Rhine water enters the North Sea, its sharp salinity gradient along the Dutch coast forms a front that guides a northeastward extension of the freshwater plume along the coastline, which is further strengthened by river runoff by other rivers (e.g., Ems, Wesser, and Elbe) along its pathway. In the German Bight, the Elbe River outflow contributes to a second gradient in the salinity front that remarkably modulates sediment dynamics in the HMA (Figure 9). The salinity front is persistently located above the HMA with minor seasonal fluctuations associated with variation in the river runoff and wind direction. By contrast, the tidal mixing front forms and crosses the HMA mainly during summer and diminishes or disappears in winter, causing a seasonal variability in the sediment trapping efficiency and deposition in the HMA. The tidal mixing front leads to the development of cyclonic and anticyclonic flows in the vertical plane, enhancing vertical exchange of SPM between surface and bottom water (Figure S4 in Supporting Information S1). It further enhances bottom shear stress in the western side of the HMA, causing a positive correlation between stratification intensity and bottom shear stress that is opposite to that related to the salinity front as shown in Figure 11. This also accounts for a reduced sediment deposition in the HMA in summer compared to in winter.

4.2. Major Sediment Source for the HMA

Our results suggest that HMA is naturally mainly fed by sediment inflows from its western and southern boundary (Figure 8). This indicates the paleo-Elbe Valley and the southwestern coasts as important sediment sources of HMA, while direct riverine sediment outflow from the Elbe River does not significantly contribute to the nowadays sedimentation in the HMA. In the Elbe and Weser River mouths, the depth-averaged residual sediment transport is directed toward inland, suggesting sediment entrapment within the estuaries. This is consistent with the study of Becherer et al. (2016), which indicates that the net sediment transport in the tidal inlet is dominated by tidal pumping during calm conditions while strong landward SPM flux is driven by advection during windy periods.

Our analysis indicates that approximately 0.8 Mt of sediment is deposited in the HMA annually (Figure 8). This is comparable to the amount of sediment delivered from the upstream River Elbe to its estuary (Irion et al., 1987). However, existing studies show that the majority of riverine sediment settles within the estuary and only particles with settling velocities less than 0.3 mm/s can be transported to the open North Sea by the freshwater plume (Rolinski, 1999; see also Figure S6 in Supporting Information S1). Therefore, direct sediment outflow from the River Elbe is far from being sufficient to supply the annual deposition in the HMA.

According to Desmit et al. (2024), the maximum coastal SPM concentration and deposition occur in the offshore transition zone, particularly at depths below 20 m in the southern North Sea and the English Channel. The 20 m-isobath was proposed as the "line of no return" beyond which particles escape coastal trapping mechanisms (Postma, 1984). In the HMA, the net sediment transport direction is jointly driven by advection following the Jutland Current, tidal pumping due to the ebb-flood asymmetries directed to southeast (Figure S5 in Supporting Information S1), and circular motions above the HMA. Sedimentation in the HMA, which sits across the 20-m isobath makes the "line of no return" less representative in the German Bight. Based on our results, the overall

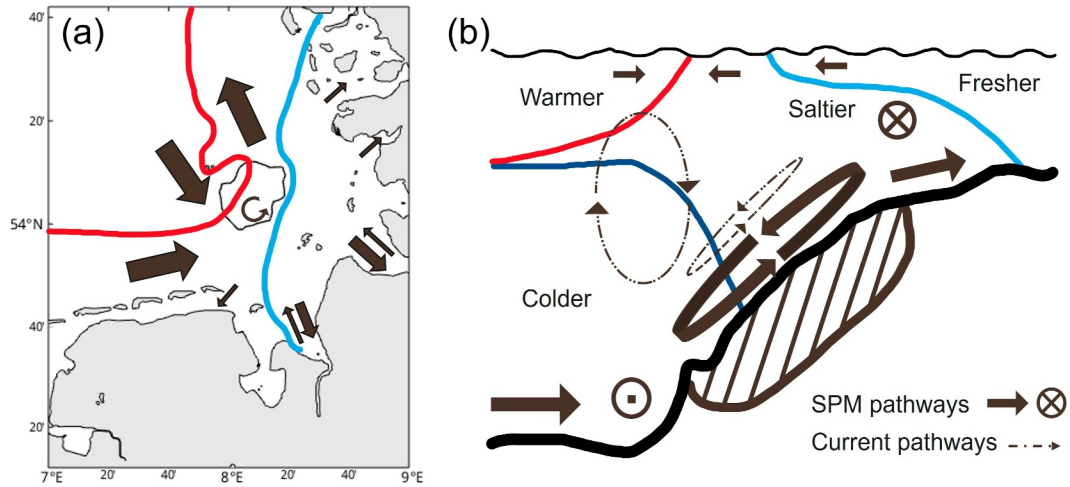

Figure 12. Sketches illustrating the depth-averaged net sediment transport pathways (larger arrows referring to larger magnitude of transport flux) associated with sedimentation in the HMA in the horizontal plane (a) and vertical plane (b). The red and blue lines indicate the mean position of the tidal mixing front and the salinity front, respectively.

transport patterns and related mechanisms for sediment transport, trapping, and deposition in the HMA can be summarized in the sketches in Figure 12.

4.3. Impact of Extreme Events

Episodic but high-flux extreme events exert considerable influence in mud depocenter development (Porz et al., 2021; W. Zhang et al., 2016). Flood events directly influence stratification and the frontal systems in the German Bight. Previous studies have demonstrated that the Elbe River flood event in June 2013 exemplifies an extreme hydrological condition (Chegini et al., 2020; Kerimoglu et al., 2020; Voynova et al., 2017). Observation data (Figure S2 in Supporting Information S1) show that the Elbe River discharge exceeded 4,000 $m^3\ s^{-1}$ on June 11th and 12th, 2013, being 5 times of its multiyear averaged runoff (860 $m^3\ s^{-1}$) recorded at the Neu Darchau gauge. By contrast, the maximum runoff in 2014 was 805 $m^3\ s^{-1}$ (occurred on 31 October), with a peak of 796 m^3/s during June 2014. The flood event in June 2013 had a significant impact on the biogeochemistry of the Elbe estuary and stratification in the southeastern German Bight with a long-lasting effect that is still observable 2 months after the event (Voynova et al., 2017). Chegini et al. (2020) found that the strong stratification near Helgoland during the summer of 2013 was primarily associated with the salinity gradient. Stratification in the HMA was more dynamic than a persistent thermal stratification in the deeper region along the paleo-Elbe Valley. Our result is able to reproduce the dynamic response of the frontal systems to the river flood (Figures 8 and 9). The SPM concentration during and after the flood event was higher than in normal periods. As a consequence, more sediment is deposited in the HMA in 2013 summer than in 2014 summer, as shown in Figure 4. This suggests an enhancement of sediment deposition in the HMA by river floods.

Wind plays a crucial role in controlling vertical circulation (Purkiani et al., 2016) and lateral advection (Becherer et al., 2016). It was suggested by Schrum (1997) that minimal stratification occurs in the German Bight under prevailing southwesterly or southerly winds, while northeasterly winds induce maximum stratification. The southwesterly winds constrained the river plume to near the shore, while northerly winds spread the plume from the shallow areas toward the paleo-Elbe valley promoting stratification (Dippner, 1998; Schrum, 1997). With regard to sediment dynamics, southwesterly winds enhance erosion, whereas northerly winds enhance net deposition through a control of stratification. This is confirmed by our correlation analysis (Figure 11) indicating that southwesterly winds have the most influential impact on bottom shear stress and sediment erosion in the HMA among all wind directions.

A notable example of an extreme wind event is Storm Xaver, which occurred in December 2013. This storm was also identified in the atmospheric forcing data set (coastDat-3) using the criteria (a) above the 95th percentile of wind speed, (b) absolute wind speed >20 m s^{-1}, and (c) duration of longer than 24 hr. We compared the simulation results before and after the storm. Results show that the strong geostrophic winds from northwest

associated with Storm Xaver have two significant impacts on sediment dynamics in the German Bight, namely increased bottom shear stress that triggers massive sediment resuspension and redistribution in nearshore shallow regions and enhanced sediment deposition in the HMA (Figure S7 in Supporting Information S1). This contributes to a higher sedimentation in winter of 2014 (December 2013–February 2014) than the previous winter (December 2012–February 2013) as shown in Figure 4. Dangendorf et al. (2016) noted that the strong northwesterly wind during Storm Xaver pushed the water toward the coast, causing exceptionally high water levels in the coastal part of the German Bight. The generated pressure gradient intensified bottom transport from southwest toward northeast. Additionally, the northwesterly winds pushed the river plume toward the paleo-Elbe Valley and the southern coastline, resulting in a southeastward shift of the salinity front that further facilitated sediment trapping within the HMA. Enhanced SPM supply caused by storm erosion in shallow coastal zones toward the HMA during the winter of 2014 was remarkably high, with net sediment deposition in the HMA almost three times of that in the winter of 2013. This highlights the role of extreme wind events like Storm Xaver in shaping sediment transport and deposition patterns in high-energy shelf seas.

4.4. Impact of Anthropogenic Activities

In addition to natural processes, anthropogenic activities such as bottom trawling, dredging, and dumping are very intensive in the North Sea (Irion et al., 1987; von Haugwitz et al., 1988; Zhang et al., 2024). These activities lead to massive sediment resuspension, transport, and redistribution (Porz et al., 2024). Dumping activities in the Wadden Sea and surrounding areas, particularly in locations close to and in the HMA, can remarkably impact the sediment budget within the HMA (Müller et al., 2024). Boxberg et al. (2020) suggested that most of the material dumped close to the HMA does not enter the eddy-controlled depositional system of the HMA. On the other hand, our simulation indicates a net sediment input from the southern and the western boundaries of the HMA. This implies that if dumping sites are located south or west of the HMA, they may contribute to the accumulation in the HMA.

Additionally, construction of dams and dredging activities in the estuaries and the Wadden Sea have reduced riverine sediment output from the rivers to the open North Sea. According to Rovira et al. (2014), the sediment budget and estuary dynamics of the Elbe River have been significantly affected by a construction of the Geesthacht Weir located ∼140 km upstream from the river mouth, with enhanced tidal pumping transporting large amounts of sediment landward (Freitag et al., 2007). However, impacts of anthropogenic activities were not considered in our model; therefore, it remains still unclear how they influence long-term sedimentation dynamics in the HMA. Further research is needed to address this knowledge gap.

4.5. Implications for Mud Depocenters in Global Shelf Seas

The complex nature of mud depocenters has been demonstrated in existing literature. Density fronts, boundaries between opposing currents, meso- and submesoscale eddies have been proposed as the major causes for formation and development of mud depocenters in high-energy shelf seas (Castaing et al., 1999; Geyer et al., 2004; Hanebuth et al., 2015; Liu et al., 2018; Xu et al., 2023; W. Zhang et al., 2016).

Our study in the HMA confirms the importance of fronts in controlling deposition of fine-grained sediment under high-energy hydrodynamic conditions. Similar mechanisms were also found from other shelf seas to explain the formation of mud depocenters there, such as the Amazon shelf (Geyet al., 2004), the Bay of Biscay (Castaing et al., 1999), the East China Sea (Xu et al., 2023) and the Iberian shelf (W. Zhang et al., 2016). Despite a similar importance of fronts, the impacts of fronts in our study area differ from other areas due to the interaction of two distinct and seasonally shifting frontal systems. Unlike the Amazon shelf, the Bay of Biscay or the East China Sea where a stable thermohaline front persists at a certain depth range year-round, the HMA is featured by a relatively stable salinity front and a seasonally variable tidal mixing front. The latter forms and migrates across the HMA during summer, then diminishes in winter, directly influencing sediment trapping efficiency and deposition patterns. This seasonal shift creates complex hydrodynamic interactions, with cyclonic and anticyclonic circulations enhancing SPM exchange and increasing bottom shear stress on the western HMA. Consequently, the sediment deposition pattern exhibits a distinct seasonal variation in the HMA.

The variability in stratification introduces a dynamic control on sediment deposition that is less commonly observed in other mud depocenters. A deepened understanding of such variability and impact on sedimentation

dynamics helps bridge the scales between short-term processes and long-term development of mud depocenters in shelf seas.

5. Conclusions

Our study aims to address the knowledge gap in understanding spatiotemporal variability of localized mud depocenters in high-energy coastal environments.

Through a detailed investigation of sediment dynamics associated with a localized mud depocenter in the southern North Sea, we found that an interplay between the wind-driven coastal circulation and two frontal systems, namely a salinity front mainly located in the shoreward part and a tidal mixing front in the seaward part of the depocenter, acts as an efficient mechanism for sediment trapping. The salinity front is persistently located above the depocenter with minor fluctuations associated with variation in the river runoff and wind direction. By contrast, the seasonal tidal mixing front forms and crosses the depocenter mainly during summer and diminishes or disappears in winter, causing a seasonal variability in the sediment trapping efficiency and the deposition rate. The presence of the tidal mixing front enhances bottom shear stress in the seaward part of the depocenter and limits sediment deposition, an opposite effect to that by the salinity front, which promotes sediment deposition. Such seasonal variability in the interplay leads to a higher sedimentation rate in the depocenter in winter than summer seasons.

Wind direction also plays an important role in driving sediment dynamics, with southwesterly winds enhancing erosion and northerly winds promoting deposition in the depocenter. Short-term extreme events such as the Elbe River flood in June 2013 and Storm Xaver in December 2013 increase sedimentation in the depocenter, contributing a considerable portion of the total annual net deposition.

The mud depocenter is naturally mainly fed by sediment from offshore and along the southern North Sea coastline. By contrast, direct riverine sediment outflow from the Elbe River plays a minor role in nowadays sedimentation in the depocenter due to a net landward transport in the estuary. On the other hand, sediment dynamics and development of mud depocenters in coastal zones are subject to influence of intensive anthropogenic activities, the impacts of which remain largely underexplored. Further research is needed to close this knowledge gap.

Data Availability Statement

SCHISM (Semi-implicit Cross-scale Hydroscience Integrated System Model) is an open-source model and distributed with an open-source Apache v2 license (Y. J. Zhang et al., 2016). Software access and licences are available from the https://doi.org/10.5281/zenodo.6537526. Figures were made with matlab R2024b-gcc-13.3.0 through the German Climate Computing Centre (DKRZ) platform. Maps were created using the mapping package M_Map (Pawlowicz, 2020) available online at www.eoas.ubc.ca/~rich/map.html. The model data supporting the conclusions of this article and matlab scripts associated with this manuscript for the calculation are published on Zenodo: https://doi.org/10.5281/zenodo.15356640.

Acknowledgments
This study is a contribution to the project "Anthropogenic impacts on particulate organic carbon cycling in the North Sea (APOC)" funded by the German Federal Ministry of Education and Research (BMBF) within the MARE:N program under Grants 03F0874C and 03F0874A. It receives support from Germany's Excellence Strategy Cluster of Excellence (Grant EXC-2077-390741603). It is also supported by the Helmholtz research program POF IV "The Changing Earth–Sustaining our Future" within "Topic 4: Coastal zones at a time of global change." This work used resources of the German Climate Computing Centre (DKRZ) granted by its Scientific Steering Committee (WLA) under project ID bg1244. We appreciate the constructive comments and suggestions from the reviewers and the editor which helped improve our study. We thank the captains, crew, and scientific teams on board RV Heincke cruise HE595 (Grant HE-595) for their technical and scientific support. Open Access funding enabled and organized by Projekt DEAL.

References

Abril, G., Nogueira, M., Etcheber, H., Cabeçadas, G., Lemaire, E., & Brogueira, M. (2002). Behaviour of organic carbon in nine contrasting European estuaries. *Estuarine, Coastal and Shelf Science*, *54*(2), 241–262. https://doi.org/10.1006/ecss.2001.0844

Addison, J. A., Finney, B. P., Jaeger, J. M., Stoner, J. S., Norris, R. D., & Hangsterfer, A. (2013). Integrating satellite observations and modern climate measurements with the recent sedimentary record: An example from Southeast Alaska. *Journal of Geophysical Research: Oceans*, *118*(7), 3444–3461.

Becherer, J., Flöser, G., Umlauf, L., & Burchard, H. (2016). Estuarine circulation versus tidal pumping: Sediment transport in a well-mixed tidal inlet. *Journal of Geophysical Research: Oceans*, *121*(8), 6251–6270. https://doi.org/10.1002/2016jc011640

Becker, G. A., Dick, S., & Dippner, J. W. (1992). Hydrography of the German bight. *Marine Ecology Progress Series*, 9–18.

Bockelmann, F.-D., Puls, W., Kleeberg, U., Müller, D., & Emeis, K.-C. (2018). Mapping mud content and median grain-size of North Sea sediments–A geostatistical approach. *Marine Geology*, *397*, 60–71. https://doi.org/10.1016/j.margeo.2017.11.003

Boxberg, F., Asendorf, S., Bartholomä, A., Schnetger, B., de Lange, W. P., & Hebbeln, D. (2020). Historical anthropogenic heavy metal input to the south-eastern North Sea. *Geo-Marine Letters*, *40*(2), 135–148. https://doi.org/10.1007/s00367-019-00592-0

Boyer, T. P., García, H. E., Locarnini, R. A., Zweng, M. M., Mishonov, A. V., Reagan, J. R., et al. (2018). World Ocean atlas 2018. https://www.ncei.noaa.gov/archive/accession/NCEI-WOA18

Burchard, H., Schuttelaars, H. M., & Ralston, D. K. (2018). Sediment trapping in estuaries. *Annual Review of Marine Science*, *10*(1), 371–395. https://doi.org/10.1146/annurev-marine-010816-060535

Castaing, P., Froidefond, J. M., Lazure, P., Weber, O., Prud'homme, R., & Jouanneau, J. M. (1999). Relationship between hydrology and seasonal distribution of suspended sediments on the continental shelf of the Bay of Biscay. *Deep Sea Research Part II: Topical Studies in Oceanography*, *46*(10), 1979–2001. https://doi.org/10.1016/S0967-0645(99)00052-1

Chegini, F., Holtermann, P., Kerimoglu, O., Becker, M., Kreus, M., Klingbeil, K., et al. (2020). Processes of stratification and destratification during an extreme river discharge event in the German Bight ROFI. *Journal of Geophysical Research: Oceans*, *125*(8), e2019JC015987. https://doi.org/10.1029/2019jc015987

Collins, A., Pulley, S., Foster, I. D., Gellis, A., Porto, P., & Horowitz, A. (2017). Sediment source fingerprinting as an aid to catchment management: A review of the current state of knowledge and a methodological decision-tree for end-users. *Journal of Environmental Management*, *194*, 86–108. https://doi.org/10.1016/j.jenvman.2016.09.075

Courant, R., Friedrichs, K., & Lewy, H. (1928). Über die partiellen Differenzengleichungen der mathematischen Physik. *Mathematische Annalen*, *100*(1), 32–74. https://doi.org/10.1007/bf01448839

Dangendorf, S., Arns, A., Pinto, J. G., Ludwig, P., & Jensen, J. (2016). The exceptional influence of storm "Xaver"on design water levels in the German Bight. *Environmental Research Letters*, *11*(5), 054001. https://doi.org/10.1088/1748-9326/11/5/054001

Desmit, X., Schartau, M., Riethmüller, R., Terseleer, N., Van der Zande, D., & Fettweis, M. (2024). The transition between coastal and offshore areas in the North Sea unraveled by suspended particle composition. *Science of the Total Environment*, *915*, 169966. https://doi.org/10.1016/j.scitotenv.2024.169966

Dick, S., Kleine, E., Müller-Navarra, S. H., Klein, H., & Komo, H. (2020). *The operational circulation model of BSH (BSHcmod): Model description and validation*. Bundesamt für Seeschifffahrt und Hydrographie Hamburg.

Dippner, J. W. (1998). Vorticity analysis of transient shallow water eddy fields at the river plume front of the River Elbe in the German Bight. *Journal of Marine Systems*, *14*(1–2), 117–133. https://doi.org/10.1016/s0924-7963(97)00008-0

Dong, J., Li, A., Liu, X., Wan, S., Xu, F., & Shi, X. (2020). Holocene climate modulates mud supply, transport, and sedimentation on the East China Sea shelf. *Journal of Geophysical Research: Earth Surface*, *125*(10), e2020JF005731. https://doi.org/10.1029/2020jf005731

Durrieu De Madron, X., Abassi, A., Heussner, S., Monaco, A., Aloisi, J. C., Radakovitch, O., et al. (2000). Particulate matter and organic carbon budgets for the Gulf of Lions (NW Mediterranean). *Oceanologica Acta*, *23*(6), 717–730. https://doi.org/10.1016/s0399-1784(00)00119-5

FGG, E. (2024). FGG Elbe database. (Flussgebietsgemeinschaft Elbe/Elbe River Basin Association) www.fgg-elbe.de

Freitag, C., Ohle, N., Strotmann, T., & Glindemann, H. (2007). Concept of a sustainable development of the Elbe estuary. In *River, Coastal and Estuarine Morphodynamics: RCEM* (pp. 1085–1092). Taylor and Francis.

Geyer, W. R., Hill, P. S., & Kineke, G. C. (2004). The transport, transformation and dispersal of sediment by buoyant coastal flows. *Continental Shelf Research*, *24*(7–8), 927–949. https://doi.org/10.1016/j.csr.2004.02.006

Glorioso, P., & Simpson, J. (1994). Numerical modelling of the M2 tide on the northern Patagonian Shelf. *Continental Shelf Research*, *14*(2–3), 267–278. https://doi.org/10.1016/0278-4343(94)90016-7

Hafen, H., & Nach Neßsand, U. V. B. (2013). Umgang mit Baggergut aus dem.

Hafen, H., & nach Neßsand, U. V. B. (2014). Umgang mit Baggergut aus dem.

Hanebuth, T. J. J., Lantzsch, H., & Nizou, J. (2015). Mud depocenters on continental shelves—Appearance, initiation times, and growth dynamics. *Geo-Marine Letters*, *35*(6), 487–503. https://doi.org/10.1007/s00367-015-0422-6

Hebbeln, D., Scheurle, C., & Lamy, F. (2003). Depositional history of the Helgoland mud area, German Bight, North Sea. *Geo-Marine Letters*, *23*(2), 81–90. https://doi.org/10.1007/s00367-003-0127-0

Helmholtz-Zentrum Geesthacht, Z. F. M.-U. K. G. H. (2017). *CoastDat-3_COSMO-CLM_ERAi [World Data Center for Climate]*. http://cera-www.dkrz.de/WDCC/ui/Compact.jsp?acronym=coastDat-3_COSMO-CLM_ERAi

Hofmeister, R., Flöser, G., & Schartau, M. (2017). Estuary-type circulation as a factor sustaining horizontal nutrient gradients in freshwater-influenced coastal systems. *Geo-Marine Letters*, *37*(2), 179–192. https://doi.org/10.1007/s00367-016-0469-z

Holt, J., & Umlauf, L. (2008). Modelling the tidal mixing fronts and seasonal stratification of the Northwest European Continental shelf. *Continental Shelf Research*, *28*(7), 887–903. https://doi.org/10.1016/j.csr.2008.01.012

ICES Dataset on Ocean Hydrography. (2014). The international council for the exploration of the sea, Copenhagen. Retrieved from http://geo.ices.dk

Irion, G., Wunderlich, F., & Schwedhelm, E. (1987). Transport of clay minerals and anthropogenic compounds into the German Bight and the provenance of fine-grained sediments SE of Helgoland. *Journal of the Geological Society*, *144*(1), 153–160. https://doi.org/10.1144/gsjgs.144.1.0153

Jokinen, S. A., Virtasalo, J. J., Kotilainen, A. T., & Saarinen, T. (2015). Varve microfabric record of seasonal sedimentation and bottom flow-modulated mud deposition in the coastal northern Baltic Sea. *Marine Geology*, *366*, 79–96. https://doi.org/10.1016/j.margeo.2015.05.003

Kämpf, J. (2019). Extreme bed shear stress during coastal downwelling. *Ocean Dynamics 2019*, *69*(5), 581–597. https://doi.org/10.1007/s10236-019-01256-4

Kerimoglu, O., Voynova, Y. G., Chegini, F., Brix, H., Callies, U., Hofmeister, R., et al. (2020). Interactive impacts of meteorological and hydrological conditions on the physical and biogeochemical structure of a coastal system. *Biogeosciences*, *17*(20), 5097–5127. https://doi.org/10.5194/bg-17-5097-2020

Kossack, J., Mathis, M., Daewel, U., Zhang, Y. J., & Schrum, C. (2023). Barotropic and baroclinic tides increase primary production on the Northwest European Shelf. *Frontiers in Marine Science*, *10*, 1206062. https://doi.org/10.3389/fmars.2023.1206062

Lenz, N., Spiegel, T., Hathorne, E., Wallmann, K., Eisenhauer, A., & Frank, M. (2024). Provenance of clay-sized detrital sediments in the North Sea and the Skagerrak region based on radiogenic Nd-Sr-Hf isotopes and clay mineral compositions: Assessing the impact of coastal and seabed erosion. *Frontiers in Marine Science*, *11*, 1416519. https://doi.org/10.3389/fmars.2024.1416519

Liu, J. T., Hsu, R. T., Yang, R. J., Wang, Y. P., Wu, H., Du, X., et al. (2018). A comprehensive sediment dynamics study of a major mud belt system on the inner shelf along an energetic coast. *Scientific Reports 2018*, *8*(1), 4229. https://doi.org/10.1038/s41598-018-22696-w

Locarnini, R. A., Mishonov, A. V., Baranova, O. K., Boyer, T. P., Zweng, M. M., García, H. E., et al. (2019). World Ocean Atlas 2018, volume 1: Temperature.

Lyard, F. H., Allain, D. J., Cancet, M., Carrère, L., & Picot, N. (2021). FES2014 global ocean tide atlas: Design and performance. *Ocean Science*, *17*(3), 615–649. https://doi.org/10.5194/os-17-615-2021

Ma, M., Porz, L., Schrum, C., & Zhang, W. (2024). Physical mechanisms, dynamics and interconnections of multiple estuarine turbidity maximum in the Pearl River estuary. *Frontiers in Marine Science*, *11*, 1385382. https://doi.org/10.3389/fmars.2024.1385382

Mayer, B. (1995). *Ein dreidimensionales, numerisches Schwebstoff-Transportmodell mit Anwendung auf die Deutsche Bucht*. Dissertation zur Erlangung des Doktorgrades der Naturwissenschaften im Fachbereich Geowissenschaften der Universität Hamburg.

Müller, D., Liu, B., Geibert, W., Holtappels, M., Sander, L., Miramontes, E., et al. (2024). *Depositional controls and budget of organic carbon burial in fine-grained sediments of the North Sea–the Helgoland Mud Area as a test field* (pp. 1–37). EGUsphere, 2024.

Pache, T., Brockamp, O., & Clauer, N. (2008). Varied pathways of river-borne clay minerals in a near-shore marine region: A case study of sediments from the Elbe-and Weser rivers, and the SE North Sea. *Estuarine, Coastal and Shelf Science*, *78*(3), 563–575. https://doi.org/10.1016/j.ecss.2008.01.016

Pawlowicz, R. (2020). M_Map: A mapping package for matlab. Computer Software.

Pinto, L., Fortunato, A., Zhang, Y., Oliveira, A., & Sancho, F. (2012). Development and validation of a three-dimensional morphodynamic modelling system for non-cohesive sediments. *Ocean Modelling*, *57*, 1–14. https://doi.org/10.1016/j.ocemod.2012.08.005

Porz, L., Zhang, W., Christiansen, N., Kossack, J., Daewel, U., & Schrum, C. (2024). Quantification and mitigation of bottom-trawling impacts on sedimentary organic carbon stocks in the North Sea. *Biogeosciences*, *21*(10), 2547–2570. https://doi.org/10.5194/bg-21-2547-2024

Porz, L., Zhang, W., Hanebuth, T. J. J., & Schrum, C. (2021). Physical processes controlling mud depocenter development on continental shelves – Geological, oceanographic, and modeling concepts. *Marine Geology*, *432*, 106402. https://doi.org/10.1016/j.margeo.2020.106402

Postma, H. (1984). *Introduction to the symposium on organic matter in the Wadden Sea* (Vol. 10, pp. 15–22). Netherlands Institute for Sea Research Publication Series.

Purkiani, K., Becherer, J., Klingbeil, K., & Burchard, H. (2016). Wind-induced variability of estuarine circulation in a tidally energetic inlet with curvature. *Journal of Geophysical Research: Oceans*, *121*(5), 3261–3277. https://doi.org/10.1002/2015jc010945

Ralston, D. K., Geyer, W. R., & Warner, J. C. (2012). Bathymetric controls on sediment transport in the Hudson River estuary: Lateral asymmetry and frontal trapping. *Journal of Geophysical Research*, *117*(C10). https://doi.org/10.1029/2012jc008124

Ricker, M., Meyerjürgens, J., Badewien, T. H., & Stanev, E. V. (2021). Lagrangian methods for visualizing and assessing frontal dynamics of floating marine litter with a focus on tidal basins. *Chemical Oceanography of Frontal Zones*, 407–442. https://doi.org/10.1007/698_2021_812

Rolinski, S. (1999). On the dynamics of suspended matter transport in the tidal river Elbe: Description and results of a Lagrangian model. *Journal of Geophysical Research*, *104*(C11), 26043–26057. https://doi.org/10.1029/1999jc900230

Rovira, A., Ballinger, R., Ibáñez, C., Parker, P., Dominguez, M. D., Simon, X., et al. (2014). Sediment imbalances and flooding risk in European deltas and estuaries. *Journal of Soils and Sediments*, *14*(8), 1493–1512. https://doi.org/10.1007/s11368-014-0914-4

Samuelsen, A., Schrum, C., Yumruktepe, V. Ç., Daewel, U., & Roberts, E. M. (2022). Environmental change at deep-sea sponge habitats over the last half century: A model hindcast study for the age of anthropogenic climate change. *Frontiers in Marine Science*, *9*, 737164. https://doi.org/10.3389/fmars.2022.737164

Schrum, C. (1997). Thermohaline stratification and instabilities at tidal mixing fronts: Results of an eddy resolving model for the German Bight. *Continental Shelf Research*, *17*(6), 689–716. https://doi.org/10.1016/s0278-4343(96)00051-9

Severinghaus, J. P., & Brook, E. J. (1999). Abrupt climate change at the end of the last glacial period inferred from trapped air in polar ice. *Science*, *286*(5441), 930–934. https://doi.org/10.1126/science.286.5441.930

Shi, Y., Gao, J., Sheng, H., Du, J., Jia, J., Wang, Y., et al. (2019). Cross-front sediment transport induced by quick oscillation of the Yellow Sea warm current: Evidence from the sedimentary record. *Geophysical Research Letters*, *46*(1), 226–234. https://doi.org/10.1029/2018gl080751

Sievers, J., Malte, R., & Milbradt, P. (2020). EasyGSH-DB: Subject area—sedimentology [Dataset]. https://doi.org/10.48437/02.2020.K2.7000.0005

Simpson, J. H., & Hunter, J. (1974). Fronts in the Irish Sea. *Nature*, *250*(5465), 404–406. https://doi.org/10.1038/250404a0

Song, Y., & Haidvogel, D. (1994). A semi-implicit ocean circulation model using a generalized topography-following coordinate system. *Journal of Computational Physics*, *115*(1), 228–244. https://doi.org/10.1006/jcph.1994.1189

Sprenk, D., Weber, M., Kuhn, G., Wennrich, V., Hartmann, T., & Seelos, K. (2014). *Seasonal changes in glacial polynya activity inferred from Weddell Sea varves*. Palaeoclimate and Ice-Sheet Dynamics in the Southern Ocean.

Stanev, E. V., Al-Nadhairi, R., & Valle-Levinson, A. (2015). The role of density gradients on tidal asymmetries in the German Bight. *Ocean Dynamics*, *65*(1), 77–92. https://doi.org/10.1007/s10236-014-0784-8

Timko, P. G., Arbic, B. K., Hyder, P., Richman, J. G., Zamudio, L., O'Dea, E., et al. (2019). Assessment of shelf sea tides and tidal mixing fronts in a global ocean model. *Ocean Modelling*, *136*, 66–84. https://doi.org/10.1016/j.ocemod.2019.02.008

Tippenhauer, S. (2022). CTD processing report of RV Heincke HE597.

Tonani, M., Sykes, P., King, R. R., McConnell, N., Péquignet, A.-C., O'Dea, E., et al. (2019). The impact of a new high-resolution ocean model on the Met Office North–West European Shelf forecasting system. *Ocean Science*, *15*(4), 1133–1158. https://doi.org/10.5194/os-15-1133-2019

von Haugwitz, W., Wong, H. K., & Salge, U. (1988). The mud area southeast of Helgoland: A reflection seismic study. *Mitteilungen aus dem Geologisch-Palaontologischen Institut der Universitat Hamburg*, *65*, 409–422.

Voynova, Y. G., Brix, H., Petersen, W., Weigelt-Krenz, S., & Scharfe, M. (2017). Extreme flood impact on estuarine and coastal biogeochemistry: The 2013 Elbe flood. *Biogeosciences*, *14*(3), 541–557. https://doi.org/10.5194/bg-14-541-2017

Walsh, J. P., & Nittrouer, C. (1999). Observations of sediment flux to the Eel continental slope, northern California. *Marine Geology*, *154*(1–4), 55–68. https://doi.org/10.1016/s0025-3227(98)00103-0

Warner, J. C., Sherwood, C. R., Signell, R. P., Harris, C. K., & Arango, H. G. (2008). Development of a three-dimensional, regional, coupled wave, current, and sediment-transport model. *Computers & Geosciences*, *34*(10), 1284–1306. https://doi.org/10.1016/j.cageo.2008.02.012

Weight, R. W. R., Anderson, J. B., & Fernandez, R. (2011). Rapid mud accumulation on the central Texas shelf linked to climate change and sea-level rise. *Journal of Sedimentary Research*, *81*(10), 743–764. https://doi.org/10.2110/jsr.2011.57

Weilbeer, H. (2014). Sediment transport and sediment management in the Elbe estuary. *Die Kuste*, *81*, 409–426.

Weltje, G. J., & Brommer, M. B. (2011). Sediment-budget modelling of multi-sourced basin fills: Application to recent deposits of the western Adriatic mud wedge (Italy). *Basin Research*, *23*(3), 291–308. https://doi.org/10.1111/j.1365-2117.2010.00484.x

Winterwerp, J., Van Kesteren, W., Van Prooijen, B., & Jacobs, W. (2012). A conceptual framework for shear flow–induced erosion of soft cohesive sediment beds. *Journal of Geophysical Research*, *117*(C10). https://doi.org/10.1029/2012jc008072

WSV. (2023). Waterways and shipping authority: Tide gauge; Alte weser lighthouse. Retrieved from https://emodnet.ec.europa.eu/geoviewer/

Xu, G., Bi, S., Gugliotta, M., Liu, J., & Liu, J. P. (2023). Dispersal mechanism of fine-grained sediment in the modern mud belt of the East China Sea. *Earth-Science Reviews*, *240*, 104388. https://doi.org/10.1016/j.earscirev.2023.104388

Ye, F., Zhang, Y. J., He, R., Wang, Z., Wang, H. V., & Du, J. (2019). Third-order WENO transport scheme for simulating the baroclinic eddying ocean on an unstructured grid. *Ocean Modelling*, *143*, 101466. https://doi.org/10.1016/j.ocemod.2019.101466

Zeiler, M., Milbradt, P., Plüß, A., & Valerius, J. (2014). Modelling large scale sediment transport in the German Bight (North Sea). *Die Kuste*, *81*, 369–392.

Zhang, W., Cui, Y., Santos, A. I., & Hanebuth, T. J. J. (2016a). Storm-driven bottom sediment transport on a high-energy narrow shelf (NW Iberia) and development of mud depocenters. *Journal of Geophysical Research: Oceans*, *121*(8), 5751–5772. https://doi.org/10.1002/2015JC011526

Zhang, W., Porz, L., Yilmaz, R., Wallmann, K., Spiegel, T., Neumann, A., et al. (2024). Long-term carbon storage in shelf sea sediments reduced by intensive bottom trawling. *Nature Geoscience*, *17*(12), 1–9. https://doi.org/10.1038/s41561-024-01581-4

Zhang, Y. J., Ye, F., Stanev, E. V., & Grashorn, S. (2016b). Seamless cross-scale modeling with SCHISM. *Ocean Modelling*, *102*, 64–81. https://doi.org/10.1016/j.ocemod.2016.05.002

Zhao, C., Daewel, U., & Schrum, C. (2019). Tidal impacts on primary production in the North Sea. *Earth System Dynamics*, *10*(2), 287–317. https://doi.org/10.5194/esd-10-287-2019

Zweng, M. M., Reagan, J. R., Seidov, D., Boyer, T. P., Locarnini, R. A., García, H. E., et al. (2019). World ocean atlas 2018, volume 2: Salinity.